A Section 508–conformant HTML version of this article is available at https://doi.org/10.1289/EHP7352.

Effects of Low-Dose Gestational TCDD Exposure on Behavior and on Hippocampal Neuron Morphology and Gene Expression in Mice

Talia E. Gileadi,[1] Abhyuday K. Swamy,[1] Zoe Hore,[2] Stuart Horswell,[3] Jacob Ellegood,[4] Conor Mohan,[1] Keiko Mizuno,[5] Anne-Katrine Lundebye,[6] K. Peter Giese,[5] Brigitta Stockinger,[7] Christer Hogstrand,[8] Jason P. Lerch,[4,9,10] Cathy Fernandes,[2,11] and M. Albert Basson[1,11]

[1]Centre for Craniofacial and Regenerative Biology, King's College London, London, UK
[2]Social, Genetic & Developmental Psychiatry Centre, Institute of Psychiatry, Psychology & Neuroscience, King's College London, London, UK
[3]Department of Bioinformatics and Biostatistics, The Francis Crick Institute, London, UK
[4]Mouse Imaging Centre (MICe), Hospital for Sick Children, Toronto, Ontario, Canada
[5]Department of Basic and Clinical Neuroscience, King's College London, London, UK
[6]Institute of Marine Research, Bergen, Norway
[7]The Francis Crick Institute, London, UK
[8]Department of Nutritional Sciences, King's College London, London, UK
[9]Department of Medical Biophysics, University of Toronto, Toronto, Ontario, Canada
[10]Wellcome Centre for Integrative Neuroimaging, University of Oxford, Oxford, UK
[11]MRC Centre for Neurodevelopmental Disorders, King's College London, London, UK

Background: 2,3,7,8-tetrachlorodibenzo-*p*-dioxin (TCDD) is a persistent and toxic environmental pollutant. Gestational exposure to TCDD has been linked to cognitive and motor deficits, and increased incidence of autism spectrum disorder (ASD) traits in children. Most animal studies of these neurodevelopmental effects involve acute TCDD exposure, which does not model typical exposure in humans.

Objectives: The aim of the study was to establish a dietary low-dose gestational TCDD exposure protocol and performed an initial characterization of the effects on offspring behavior, neurodevelopmental phenotypes, and gene expression.

Methods: Throughout gestation, pregnant C57BL/6J mice were fed a diet containing a low dose of TCDD (9 ng TCDD/kg body weight per day) or a control diet. The offspring were tested in a battery of behavioral tests, and structural brain alterations were investigated by magnetic resonance imaging. The dendritic morphology of pyramidal neurons in the hippocampal Cornu Ammonis (CA)1 area was analyzed. RNA sequencing was performed on hippocampi of postnatal day 14 TCDD-exposed and control offspring.

Results: TCDD-exposed females displayed subtle deficits in motor coordination and reversal learning. Volumetric difference between diet groups were observed in regions of the hippocampal formation, mammillary bodies, and cerebellum, alongside higher dendritic arborization of pyramidal neurons in the hippocampal CA1 region of TCDD-exposed females. RNA-seq analysis identified 405 differentially expressed genes in the hippocampus, enriched for genes with functions in regulation of microtubules, axon guidance, extracellular matrix, and genes regulated by SMAD3.

Discussion: Exposure to 9 ng TCDD/kg body weight per day throughout gestation was sufficient to cause specific behavioral and structural brain phenotypes in offspring. Our data suggest that alterations in SMAD3-regulated microtubule polymerization in the developing postnatal hippocampus may lead to an abnormal morphology of neuronal dendrites that persists into adulthood. These findings show that environmental low-dose gestational exposure to TCDD can have significant, long-term impacts on brain development and function. https://doi.org/10.1289/EHP7352

Introduction

2,3,7,8-tetrachlorodibenzo-*p*-dioxin (TCDD) is a persistent organic pollutant, a member of the polychlorinated dibenzo-*p*-dioxins/furans (PCDD/F) family (Poland et al. 1976). TCDD is a byproduct of industrial processes such as the production of iron, steel, and paper pulp, and of the burning of waste (Anderson and Fisher 2002). Incidences of high release of TCDD have occurred as a result of the Seveso disaster in 1976 (Needham et al. 1999) and the use of Agent Orange during the Vietnam War (Tai et al. 2011). Human exposure occurs mainly through consumption of contaminated food and drink, with TCDD bioaccumulating in the bodies of animals due to its lipophilic properties (EFSA CONTAM Panel 2018). TCDD has a half-life of around 4–11 y in the body (Pirkle et al. 1989; Wolfe et al. 1994; Aylward and Hays 2002) and can be transferred via the placenta and breast milk to the fetus and child (Nau et al. 1986). TCDD is considered the most toxic congener of the PCDD/F family, based on *in vivo* and *in vitro* studies of toxicity to reproduction, immunotoxicity, carcinogenicity, and teratogenicity (Safe 1998). TCDD acts as a potent agonist of the aryl hydrocarbon receptor (AHR), a member of the helix-loop-helix family (Poland et al. 1976). AHR is a ligand-activated transcription factor, sensitive to multiple endogenous ligands as well as exogenous ligands including PCDD/Fs and a subset of polychlorinated biphenyls (dioxin-like, or DL-PCBs) (Landers and Bunce 1991; Bock 2019).

Studies aimed at understanding the consequences of exposure to TCDD and related compounds have identified correlations between the levels of pre- and postnatal exposure and lower neurodevelopmental, cognitive, and psychomotor scores in children (Koopman-Esseboom et al. 1996; Vreugdenhil et al. 2002; Nakajima et al. 2006; Lee et al. 2007; Park et al. 2010; Nishijo et al. 2012; Tai et al. 2013, 2016; Tran et al. 2016; Pham et al. 2019). Cognitive and motor deficits have also been identified in rodent studies of gestational TCDD exposure (Table 1) (Schantz et al. 1996; Seo et al. 1999; Hojo et al. 2002; Powers et al. 2005; Kakeyama et al. 2014). Gestational exposure to TCDD impaired spatial learning in the Morris water maze (MWM) test in rats (Zhang et al. 2018), and memory deficits in contextual fear conditioning (CFC) tests have been observed in gestationally exposed rats (Mitsui et al. 2006) and mice (Haijima et al. 2010). Other studies have found that the TCDD-exposed animals performed

Address correspondence to M. Albert Basson, Centre for Craniofacial and Regenerative Biology, King's College London, Floor 27, Guy's Hospital Tower Wing, London, UK. Email: albert.basson@kcl.ac.uk

Supplemental Material is available online (https://doi.org/10.1289/EHP7352).

The authors declare they have no actual or potential competing financial interests.

Received 1 May 2020; Revised 19 February 2021; Accepted 29 March 2021; Published 6 May 2021.

Note to readers with disabilities: *EHP* strives to ensure that all journal content is accessible to all readers. However, some figures and Supplemental Material published in *EHP* articles may not conform to 508 standards due to the complexity of the information being presented. If you need assistance accessing journal content, please contact ehponline@niehs.nih.gov. Our staff will work with you to assess and meet your accessibility needs within 3 working days.

Table 1. Summary of studies of the behavioral and neurodevelopmental effects of gestational and lactational exposure to TCDD in animal models.

Study	Model	Dosage (ng TCDD/kg body weight)	Outcome
Thiel et al. 1994	Wistar rats	300 ng on E19, then maintenance doses of 120 ng/week	Motor deficit on the rotarod.
Schantz et al. 1996	Sprague-Dawley rats	25 or 100 ng/day on E10-E16	Fewer errors in RAM working memory task.
Seo et al. 1999	Sprague-Dawley rats	100 ng/day on E10-E16	Fewer errors in RAM working memory task, deficit in visual RL, no effect on MWM and spatial RL.
Seo et al. 2000	Sprague-Dawley rats	100 or 200 ng/day on E10-E16	Fewer errors in RAM, observed only in males and only after exposure to the lower dose.
Hojo et al. 2002	Sprague-Dawley rats	20, 60, or 180 ng on E8	Sexually dimorphic effect on operant behavior.
Markowski et al. 2002	Holtzman rats	60, 180, 540 ng on E15	Non-monotonic dose-response in impairment of cued delayed alternation behavior.
Widholm et al. 2003	Sprague–Dawley rats	100 ng/day on E10-E16	Fewer errors in visual learning for males and in visual RL for females.
Powers et al. 2005	Mice	5,000 ng on E13	$AhR^{-/+}$ Females displayed increased errors in RAM, and changes in hippocampus structure.
Mitsui et al. 2006	Wistar rats	1,000 ng on E15	Sexually dimorphic effects on CFC and CREB activation in the hippocampus.
Negishi et al. 2006	Rhesus monkeys	30 or 300 ng on E20 then maintenance doses of 1.5 or 15/month	Altered social interactions.
Nishijo et al. 2007	Wistar rats	100 ng /day on E9-E19	Delayed motor development, deficit in active avoidance learning.
Haijima et al. 2010	Mice	3,000 ng on E12.5	Deficits in CFC and auditory fear conditioning.
Endo et al. 2012	Mice	600 or 3,000 ng on E12.5	Behavioral inflexibility, increased repetitive behaviors and abnormal social behavior observed in the lower dose only.
Nguyen et al. 2013a	Wistar rats	1,000 ng on E15	Sexually dimorphic effects on the structure of the medial prefrontal cortex and the superior colliculus and on putative GABAergic neurons.
Kakeyama et al. 2014	Long-Evans rats	200 or 800 ng on E15	Impaired paired-associate learning and increased anxiety-like behavior in lower dose.
Kimura et al. 2015	Mice	600 or 3,000 ng on E12.5	Disrupted dendritic branch growth and dendritic spine density in the hippocampus.
Zhang et al. 2018	Sprague-Dawley rats	200 or 800 ng/d on E8-E14	Premature motor development, and impaired spatial learning in the MWM.
Kimura and Tohyama 2018	Mice	600 or 3,000 ng on E12.5	Pup ultrasonic vocalizations altered in the higher dose.

Note: AhR, aryl hydrocarbon receptor; CFC, contextual fear conditioning; CREB, cAMP-response element binding protein; E, embryonic day; MWM, Morris water maze; RAM, radial arm maze; RL, reversal learning; TCDD, 2,3,7,8 tetrachlorodibenzo-*p*-dioxin.

better than controls in some learning tasks (Schantz et al. 1996; Seo et al. 1999, 2000; Widholm et al. 2003), and some studies identified nonmonotonic dose–response effects on learning behaviors (Seo et al. 2000; Markowski et al. 2002; Kakeyama et al. 2014). Several studies have identified motor coordination and motor development deficits in rats gestationally exposed to TCDD (Thiel et al. 1994; Nishijo et al. 2007; Zhang et al. 2018).

TCDD levels in breast milk were shown to correlate with higher scores on autism spectrum rating scales (Nishijo et al. 2014), decreased social-emotional scores (Pham et al. 2015), and language deficits (Nishijo et al. 2012; Tai et al. 2016; Pham et al. 2019), suggesting that TCDD exposure might increase the prevalence or severity of autism spectrum disorder (ASD). Both the increase in ASD traits and the language deficits were more pronounced in boys than in girls. Subtle deficits in language scores have also been noted in children prenatally exposed to PCDD/F and PCBs, with girls more prominently affected (Caspersen et al. 2016a; 2016b). Another study failed to find an association between ASD and DL-PCBs (Granillo et al. 2019), and in a study of German children, maternal PCDD/F and DL-PCBs concentrations correlated with a reduction in ASD-like traits, especially in girls (Nowack et al. 2015). Some animal studies have identified effects of gestational TCDD exposure on ASD-like behaviors (Negishi et al. 2006; Nguyen et al. 2013a), with offspring of TCDD-exposed mice displaying behavioral inflexibility, compulsive repetitive behavior, and lowered competitive dominance (Endo et al. 2012). Conversely, pups exposed with the same experimental exposure paradigm but to a higher dose did not show the social or repetitive phenotypes, but those pups did display altered ultrasonic vocalization (USV) patterns, again suggestive of a nonmonotonic dose response (Kimura and Tohyama 2018).

The mechanisms by which TCDD disrupts neurodevelopment are poorly understood. Disruption of dendritic morphology may play an important role. Expression of a constitutively activated AHR has been shown to disrupt dendritic morphology of interneurons in the olfactory bulbs (Kimura et al. 2016), cortical layer II/III neurons (Kimura et al. 2017), and pyramidal cells in the Cornu Ammonis (CA)1 region of the hippocampus (Kimura et al. 2015) in mice. Constitutive activation of AHR in the hippocampus from E14.5 resulted in longer second-order branches of CA1 neurons. Offspring of mice orally exposed to 600 ng TCDD/kg body weight (BW) at embryonic day (E) 12.5 displayed a significant increase in the length of third-order apical branches, whereas mice given a higher dose of 3,000 ng/kg BW displayed a small decrease in the length of the second-order branches (Kimura et al. 2015). These morphological changes were detected at postnatal day (PND) 14 but not in aged mice, suggesting that this was a transient effect (Kimura et al. 2015).

Dendrite morphology is an important determinant of synaptic inputs, and an abnormal morphology is expected to affect the synaptic connectivity of functional neuronal networks in the brain (Chklovskii 2004). Dendrite morphology is regulated by myriad factors extrinsic and intrinsic to the developing neuron (Dong et al. 2015; Ledda and Paratcha 2017). The cytoskeleton is formed mainly of microtubules and actin filaments, and it controls both the dendritic structure and transport of molecules and cell components along them. Factors that interact with microtubules, such as collapsin response-mediator proteins (CRMPs), can modulate dendritic morphology by regulating microtubule

dynamics (Schmidt and Strittmatter 2007). Many of the genes with well-characterized roles in axon guidance, such as semaphorins and ephrins, also have important roles in dendritic development (Dong et al. 2015; Ledda and Paratcha 2017). Gestational TCDD exposure has been shown to induce expression of the *Sema3b* and *Sema3g* genes in the olfactory bulbs in mice, suggesting that TCDD can dysregulate pathways controlling neuron morphology (Kimura et al. 2016).

Some of the variation in behavioral phenotypes observed in different studies could be due to differences in the dose of TCDD, with several studies pointing to nonmonotonic dose–response effects on behavior (Markowski et al. 2002; Kakeyama et al. 2014). The half-life of TCDD is much shorter in rodents than in humans, and subchronic TCDD exposure of rodents to 10 ng/kg BW/d has been estimated to result in a steady-state body burden of around 100 ng/kg BW (EFSA CONTAM Panel 2018). The European Food Safety Authority (EFSA) reviewed rodent studies with estimated body burdens below 100 ng TCDD/kg BW, and identified lowest observed adverse effect levels (LOAELs) and no observed adverse effect levels (NOAELs) body burdens for outcomes, including sperm production (25 ng/kg BW) (Faqi et al. 1998), balanopreputial separation (LOAEL 42–50 ng/kg BW) (Bell et al. 2007), and embryonic loss (NOAEL 9 ng/kg BW) (Li et al. 2006). Rodent studies of cognitive, motor, and ASD-like behavioral effects undertaken so far have mostly used significantly higher doses, with daily doses of >100 ng TCDD/kg BW/d, and total doses of 180 – 5,000 ng TCDD/kg BW, often given as a single dose (Table 1). Rodent studies assessing neurodevelopmental and behavioral outcomes of repeated exposure near the LOAEL and NOAEL are therefore urgently needed.

To address this need, we exposed pregnant mice to 9 ng TCDD/kg BW/d in the diet from E0.5 until 2 d after parturition, with a cumulative dose of 200 ng/kg BW. EFSA modeling would predict this exposure to result in a total body burden of 100 ng/kg BW or less (EFSA CONTAM Panel 2018). Memory, motor, and ASD-like behaviors of the offspring were assessed, and structural magnetic resonance imaging (MRI) was carried out to compare brain anatomy of TCDD-exposed and control offspring. The effects of the TCDD diet on hippocampal neuron cell morphology and gene expression were then studied to advance our understanding of the neurodevelopmental impact of gestational TCDD exposure.

Methods

Animals

C57BL/6J mice (Charles River Laboratories) were bred and maintained in the Biological Services Unit at Guy's Campus or the Institute of Psychiatry, Psychology and Neuroscience, King's College London. All procedures involving animals were approved by the King's College London Animal Welfare and Ethical Review Board (AWERB) and the UK Home Office Animals Scientific Procedures Act 1986 (Project license P8DC5B496), in accordance with the relevant guidelines and practises. All efforts were made to minimize animal suffering and to reduce the number of animals used.

Mice were housed in open-top cages (32 cm × 16 cm × 14 cm Techniplast), and given *ad libitum* access to water, and *ad libitum* access to food (PicoLab® Irradiated Rodent Diet 205053, LabDiet) except when on the TCDD or control diets. The cages contained sawdust (Litaspen premium; Datesand Ltd.), nesting (sizzlenest; Datesand Ltd.), and a cardboard shelter (LBS Biotech). The housing room was kept at an ambient temperature of 21°C (± 2°C) and at 45% humidity level. The mice were kept at a regular 12:12 light:dark schedule with white lights (270 lux) during the light cycle [from 0730 hours to 1930 hours (from 7:30 A.M. to 7:30 P.M.)] and with lights lower than 2 lux during the dark cycle [1930 hours to 0730 hours (7:30 P.M. to 7:30 A.M.)]. Mice were housed in a conventional (nonbarrier) mouse facility. Sentinel mice were negative for all Federation of Laboratory Animal Science Associations (FELASA)-relevant murine infectious agents as diagnosed by a health monitoring laboratory, Envigo, Huntingdon, UK (https://www.envigo.com/).

Gestational TCDD Exposure

Mouse TCDD and control diets were produced at the Institute of Marine Research as previously described (Maranghi et al. 2013). Briefly, the diets were prepared in accordance with the standard rodent diet formulation AIN-93G, except that freeze-dried Atlantic salmon was used as the main source of protein and fat, reflecting the fact that fatty fish are a principal source of dietary exposure to dioxins. Half of the diet was spiked with 60 pg TCDD/g feed (TRC-T291370; LGC Limited) dissolved in dimethylsulfoxide (DMSO) (C12014.2; Chiron), and the other half with equivalent DMSO volume. The final concentration of TCDD was measured as 45.5 pg/g feed in the TCDD diet and <0.29 pg/g in the control diet. The diets were irradiated and frozen at −20°C for storage. Pregnant female mice were placed on either the TCDD or the control diet from the day a plug was found (E0.5) until the litter was at PND2, and then returned to the normal diet (PicoLab® Irradiated Rodent Diet 20-5053; LabDiet). During the exposure, the dams were weighed daily and fed 20% of their BW in diet per day, resulting in an estimated dose of 9 ng/kg BW/d. Pups were weighed at PNDs 10, 21, 29–30, and 150 to assess the effect of the diets on weight.

Figure 1 summarizes the overall design of the study. All pups from each litter were used in the behavior experiments (1–6 pups per sex per litter). To limit litter effects, where possible litters were spread across end points such that 1–2 pups per litter were used in the CA1 morphology and TCDD analyses, and 1–5 pups per litter used in the MRI analysis. One litter per diet was used for the gene expression analysis.

Behavioral Testing of TCDD-Exposed and Control Mice

Mice were weaned at PND28 and then singly housed to avoid any potential confounds from social hierarchies. Although single housing in mice can be a social stressor, it has been shown to have minimal effects on the C57BL/6J strain and eliminates the potential confounds of group housing, such as the establishment of social hierarchies (Lad et al. 2010). The estrous phase of the female mice was not checked in this study, but it is unlikely that this affected the results because there were no major differences in the variance observed in the behavioral measures between males and females. Female and male mice were housed in the same room, which typically results in regular estrous cycling and synching of estrous in the females (deCatanzaro 2015). Sawdust and enrichment were changed every other week but never on the day before or the day of testing.

All testing took place during the light phase (0830 hours to 1830 hours). Although mice are nocturnal animals, previous research suggests that many behaviors are not affected by the time of the day mice are tested, but by the change in light levels, from housing to testing environments (Valentinuzzi et al. 2000; Beeler et al. 2006). Therefore, all tests were performed under standard room lighting unless stated otherwise. Behaviors were performed in soundproof rooms and recorded using a camera positioned above or next to the test arenas. When needed, the movement of each mouse was tracked using EthoVision (version

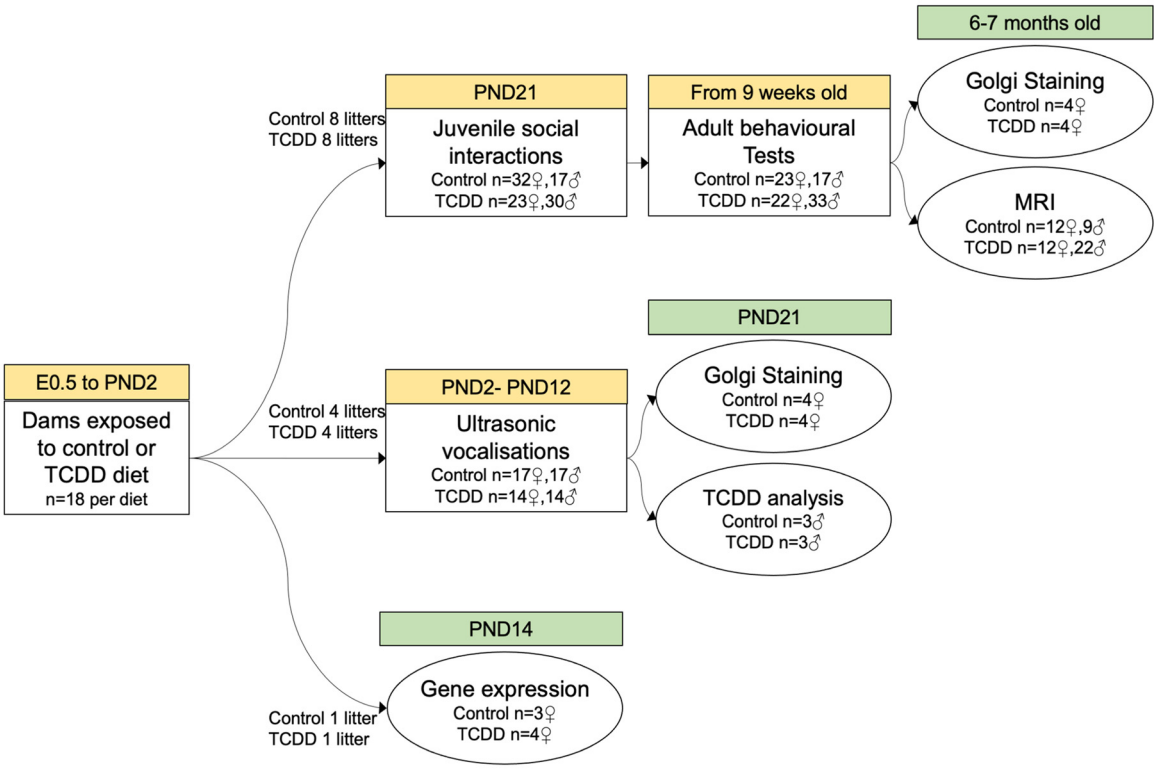

Figure 1. Summary of study design. Sample size, age and sex of mice are shown for each set of experiments. All pups from each litter were used in the behavior experiments (1–6 pups per sex per litter). Litters were spread across end points such that 1–2 pups per litter were used in the CA1 morphology and TCDD analyses, and 1–5 pups per litter were used in the MRI analysis. One litter per diet was used for the gene expression analysis. Note: E, embryonic day; MRI, magnetic resonance imaging; PND, postnatal day; TCDD, 2,3,7,8 tetrachlorodibenzo-*p*-dioxin.

9.0; Noldus Information Technologies). After each individual test, boli and urine were removed, and the test arena was cleaned with 1% Anistel® solution (Trisel Solution) to remove any odors. Experimenters were blind to the diet group of the animals both during the testing and subsequent scoring of the recorded behaviors. Testing was carried out by female experimenters.

Mice that underwent USV testing were given paw tattoos immediately after testing on PND2 to allow for identification of pups. Conspecific mice were housed in a room separate from that of the test mice to ensure the conspecifics were unfamiliar to the test mice. Test mice were never exposed to the same conspecific during testing to ensure novelty of the conspecifics.

Behavioral data was analyzed using GraphPad Prism® 8 (GraphPad Software). The effects of diet and batch on behavioral measures were tested using an unpaired Student *t*-test, a two-way or three-way analysis of variance (ANOVA) with Sidak's multiple comparisons post hoc tests. One-sample Student *t*-tests were used to determine whether behavior variables were significantly different from values expected by chance for the time in the target quadrant (MWM) and preference ratios (three chamber sociability and social novelty test). Because TCDD exposure has often been linked to sexually dimorphic effects on behavior, each sex was analyzed separately (Hojo et al. 2002; Powers et al. 2005; Mitsui et al. 2006; Nguyen et al. 2013b). $p < 0.05$ was considered significant.

Order of Tests

Mice of both sexes were tested for juvenile social interaction at PND21, with adult tests commencing once the mice reached 9 weeks of age in two batches. The behavioral tests were carried out in the following order: juvenile social interactions, light-dark box, open field, adult social interactions, self-grooming, three-chamber test, marble burying, elevated plus maze, spontaneous spatial novelty discrimination test, rotarod, grip strength, MWM, and CFC. USVs on separation from the nest were measured on a separate batch of mice.

Juvenile Social Interactions

Mice were tested for social interactions at PND21 using a protocol adapted from (McFarlane, et al. 2008). Mice were singly housed for an hour in the testing room before testing. The test mouse was placed in a clean empty cage along with a socially novel sex-matched juvenile conspecific mouse. The cage was filmed for 10 min, and social (anogenital sniffing, head sniffing, and body sniffing) and aggressive behaviors of the test mice were scored from video.

Light-Dark Box Test

The light/dark test was carried out as adapted from (Crawley and Goodwin, 1980). The arena was a 44 cm × 21 cm × 21 cm acrylic box divided into a dark chamber (15 lux) and light chamber (100 lux). The dark chamber made up a third of the total area of the box. Test mice were placed in the dark chamber and allowed to explore the box for 5 min. Avoidance of the light chamber was used as a measure of anxiety.

Open Field Test

The open field test was carried out as adapted from (Candland and Nagy 1969). Individual mice were placed in a round arena 40 cm in diameter lit at 10 lux. The movements of the mice were tracked for 10 min. A circle 20 cm in diameter at the center of the open field arena was designated the center zone, and a ring 5 cm thick around the perimeter of the arena was designated as

the outer zone. Avoidance of the center zone was used as a measure of anxiety, and total distance moved in the outer zone was used as a measure of locomotive activity level.

Adult Social Interactions

Mice were tested at 9 wk old, using a protocol adapted from McFarlane et al. (2008). Mice were singly housed for an hour in the testing room before testing. The test mouse was placed in a clean empty cage along with a socially novel sex-matched juvenile conspecific mouse. The cage was filmed for 5 min, and social (anogenital sniffing, head sniffing, and body sniffing) and aggressive behaviors of the test mice were scored from video.

Self-Grooming

Self-grooming was assessed using a protocol adapted from McFarlane et al. (2008). Individual mice were placed in an empty standard housing cage (32 cm × 16 cm × 14 cm) and given 10 mins to habituate in a dimly lit test room (<10 lux). The cumulative time spent self-grooming in the following 10 mins was scored from video.

Three-Chamber Sociability and Social Novelty Test

Individual mice were tested in the three-chamber box over three trials in a protocol adapted from Yang et al. (2011). In trial 1, the mice were habituated to the empty box over 10 min. In trial 2, an unfamiliar sex-matched juvenile conspecific mouse was placed in a wire containment cup on either the left or right chamber (counter balanced within each group), and an unfamiliar mouse-like object (tally counter, Appleton Woods GC101) was placed in a wire containment cup in the opposite chamber. Test mice could explore the box for 10 min. Social preference was measured as 100 × (time spent with novel mouse)/(time spent with novel mouse novel object). In trial 3, the unfamiliar object was replaced with a novel unfamiliar conspecific, and the test was run for another 10 min. Social novelty preference was measured as 100 × (time spent with novel mouse)/(time spent with novel mouse familiar mouse).

Marble Burying

Repetitive digging behavior was measured in a protocol adapted from (Deacon 2006), in a dimly lit (10 lux) test room. Twelve blue glass marbles were placed in a symmetrical 4 cm × 3 cm grid on top of 5 cm of deep sawdust (Litaspen premium; Datesand Ltd.) in a clean empty cage (32 cm × 16 cm × 14 cm). Each mouse was recorded for 30 mins, and the number of marbles buried was counted live at 2.5-, 5-, 7.5-, 10-, 20-, and 30-min intervals.

Elevated Plus Maze Test (EPM)

The EPM was carried out as adapted from Fernandes and File (1996). The two closed arms of the EPM were surrounded by walls and were lit at ∼10 lux, whereas the open arms had no walls and were lit at ∼100 lux. The maze was positioned 40 cm above the floor. Individual mice were placed in a closed arm, and their movements were tracked for 5 min. Avoidance of the open arms was used as a measure of anxiety.

Spontaneous Spatial Novelty Discrimination Test

The test was adapted from Bannerman et al. (2008). Testing was carried out in a Y-shaped maze with extra-maze visual cues at the end of the two arms. Each mouse was placed in the starting arm and allowed to explore the maze for 5 min, with one of the arms blocked off. The mouse was returned to its home cage for 60 min and then returned to the testing room. The blocked arm was opened and designated the "novel" arm, with the arm already explored by the mouse termed the "familiar" arm. The mouse was again placed in the starting arm and allowed to explore for 5 min, and the time spent on each arm was tracked.

Rotarod

Mice were tested in seven trials over 1 d on the rotarod in a protocol adapted from Costa et al. (2004). In each trial, the rod accelerated between 10 – 50 rpm over 300 s, and the latency to fall was recorded. The mice were allowed to rest for 5 min between each trial.

Grip Strength

Grip strength was measured three times using a Linton Grip Strength Meter (MJS Technology) and the three recordings were averaged.

MWM

Spatial memory and learning were assessed in the MWM essentially as described previously (Lad et al. 2010). Mice were tested in a circular pool 1.3 meters in diameter surrounded by four extra-maze visual cues. Four equidistant positions around the edge of the pool were designated as Target (T), Opposite (O), Left (L), and Right (R), dividing the arena into four quadrants. The mice were tested in four trials per day starting from each position in a pseudorandom order. On the first day of testing, a visible platform was placed in the T quadrant. In the acquisition stage, water was added to submerge the platform, and mice were tested in 7 consecutive hidden platform days. A probe trial was carried out after testing on the last day of acquisition. The next day, the platform was moved to the opposite quadrant, and the mice tested for reversal learning during the reversal stage. The latency to reach the platform in each trial was recorded. The time spent in the target quadrant during the probe trial was compared to the amount of time expected by chance (25%). The proportion of time the mice spent at the outer part of the pool (the outer 15-cm ring of the arena) was recorded as a measure of thigmotaxis, along with any floating behavior and the average swim velocity.

CFC

The protocol was adapted from Von Hertzen and Giese (2005). Each mouse was placed into a soundproof box with a stainless-steel metal grid floor containing a camera (MedAssociates). A white noise generator provided consistent background noise. The chamber was cleaned with 70% ethanol (101077Y; VWR), and an ethanol-soaked tissue was placed under the grid to provide an olfactory cue. Before testing, the mice were acclimatized in the testing room for at least 30 min. During training, each mouse was placed into the chamber and, after an exploratory period of 148 s, given a 0.7-mA foot shock lasting 2 s, followed by a second foot shock 30 s later. After another 30 s, the mouse was returned to its home cage. Contextual fear memory was measured 24 h later by scoring the frequency of the freezing in the chamber for 5 min. Freezing was scored manually by observing the mouse for 2 s out of every 5 s and recording freezing if no movement except respiration was observed during these 2 s.

USVs

Pups were tested as described before (Romano et al. 2013), on PND2, 4, 6, 8, 10, and 12. During testing, each pup was removed from its cage and transferred to an empty plastic container in a

sound-attenuating box. An ultrasound microphone (Avisoft UltraSoundGate condenser microphone capsule CM16; Avisoft Bioacoustics) recorded USVs for 3 min, and then the test mouse was returned to its cage. USVs were recorded using Avisoft Recorder software (version 3.2) with a sampling rate of 250 kHz, and then analyzed using Avisoft SASLab Pro (version 5.2.10). Spectrograms were generated with a fast fourier transformation (FFT), with FFT length of 1,024 points and a time window overlap of 75% (100% Frame, Hamming window). Calls were manually counted after blinding to sex and diet.

Structural MRI

Following behavioral testing, adult mice of both sexes (6–7 months old) were anesthetized by terminal intraperitoneal injection of sodium pentobarbital and intracardially perfused with 30 mL of buffer [0.1 M PBS, 10 U/mL heparin, 2 mM ProHance (0270-1111; Bracco Diagnostics Inc)], and 30 mL of paraformaldehyde (PFA) buffer [0.1 M PBS, 4% PFA (43368.9 M Alfa Aesar), 2 mM ProHance]. Following perfusion, the brains, left in the skulls, were dissected out and incubated overnight in the PFA buffer. Samples were then incubated in 0.1 M PBS with 2 mM ProHance and 0.02% sodium azide for at least a month. A multichannel 7.0 Tesla MRI scanner (Agilent Inc.) was used to image the brains within their skulls. Sixteen custom-built solenoid coils imaged the brains in parallel (Bock et al. 2005; Lerch et al. 2011). Parameters used in the anatomical MRI scans: T2-weighted 3D fast spin-echo sequence, with a cylindrical acquisition of k-space, and with a TR of 350 ms, and TEs of 12 ms per echo for 6 echoes, 2 averages, field-of-view of $20 \times 20 \times 25$ mm^3 and matrix size $= 504 \times 504 \times 630$, giving an image with 0.04 mm isotropic voxels (Spencer 2017). The current scan time required for this sequence is approximately 14 h. Deformation based morphometry was used to visualize and compare any changes in the mouse brains. First, the images were linearly (6-parameter fit followed by a 12-parameter fit) and then nonlinearly registered together. For a detailed protocol describing the registration process and lists of all the steps, please refer to Lerch et al. (2011). Then a population atlas representing the average anatomy of the entire study sample was created. All registrations were performed with a combination of mni_autoreg tools (Collins et al. 1994) and advanced normalization tools (ANTs) (Avants et al. 2008, 2011). The software used for the registration uses the Pydpiper framework (Friedel et al. 2014), and all of the registration tools can be found on GitHub at https://github.conm/Mouse-Imaging-Center. At completion of this registration, all scans had been deformed into alignment with each other in an unbiased fashion without human involvement. As with typical deformation-based morphometry, this approach allows for analysis of the deformations required to register the anatomy of each individual mouse into the final atlas space (Nieman et al. 2006; Lerch et al. 2008). The Jacobian determinants, as calculated through this analysis process, were used as measures of volume at each voxel and compared across diet groups.

Volumetric changes were calculated on a regional and a voxel-wise basis. A preexisting classified MRI atlas was registered to the population atlas to calculate regional volumes encompassing 182 different structures throughout the brain (Dorr et al. 2008; Ullmann et al. 2013; Steadman et al. 2014). Statistical analyses were applied comparing the absolute and relative volume of these 182 different regions and on a voxel-wise basis in the brains of TCDD and control mice. For this analysis, the sexes were pooled together to increase statistical power, and therefore, sex was covaried for in the linear model used to assess volumetric differences (Region/Voxel $\sim$ Diet + Sex). Relative volume was calculated by further covarying for total brain volume. Multiple comparisons were controlled for using the false discovery rate (FDR) (Genovese et al. 2002).

Morphological Analysis of CA1 Pyramidal Neurons

Female mice were culled at PND21 or 7 months old following USV or adult behavior testing, respectively. The brains were processed using the FD rapid Golgi stain kit (PK401; FD NeuroTechnologies) following the manufacturer's protocol. Briefly, animals were culled in a CO_2 chamber, and the brains were incubated in the impregnation solution for 12 d, then in solution C for 3 d at room temperature in the dark. The brains were then embedded in 4% agarose (16500500; Invitrogen) and sectioned in solution C using the vibratome Leica VT1000s (Leica Biosystems). Coronal 100-μm sections were then dried onto superfrost plus slides (631-0108P; VWR), stained and dehydrated before being cleared in xylene (16371; Alfa Aesar), and mounted in DPX mountant (100579; Merck).

Fully stained hippocampal CA1 pyramidal neurons were imaged using a 40X-S plan Flour ELWD objective on a Nikon Eclipse Ti2 Inverted Microscope with brightfield imaging on a Nikon DS-Qi2 sCMOS camera. Z-stacks with a 1.5-μm step size were taken of the entire cell. Tracing and analyzing of the dendritic arbor was done using the "Simple Neurite Tracer" plugin in FIJI (Longair et al. 2011; Schindelin et al. 2012) by investigators blind to the diet group. Dendritic spine density in adult CA1 pyramidal neurons was manually quantified using FIJI by selecting segments of apical and basal dendrites of at least 1.5 μm, excluding primary branches.

Sholl analysis was used to assess dendritic morphology by drawing concentric circles every 5 μm around the center of the cell soma and recording the number of intersections of a given circle with traced dendrites (Sholl 1953). Because basal morphology and apical morphology are very different in pyramidal cells, Sholl analysis of the apical and basal arbors was carried out separately. All analyses were performed using R (version 3.3.1; R Development Core Team). For each data set (Apical Adult, Apical PND21, Basal Adult, Basal PND21), the number of intersections was estimated by way of a Poisson generalized linear mixture model via piecewise quasi likelihood (glmmPQL). Specifically, the number.of.intersections + 1 was considered to be the dependent variable (adding one to allow for the use of a log link in the Poisson model), with independent predictors being the interaction of diet (Control/TCDD) with a cubic polynomial in the (median centered) distance. Finally, a random effect was included to correct for repeated measures from individual mice.

The final model was thus:

$$\begin{aligned} &\text{MASS::glmmPQL}((\text{number.of.intersections} + 1) \sim \\ &\quad (\text{c.dist} + \text{c.dist}^2 + \text{c.dist}^3) * \text{diet}, \\ &\text{random} = \sim 1|\text{mouse}, \ \text{family} = \text{poisson}). \end{aligned} \tag{1}$$

The order of the polynomial (cubic) was selected after consideration of residual sum of squares diagnostic plots and coefficient tables for each degree from 1 to 5. Nesting of mouse within litter was considered as a random term, but we found that the litter had negligible additional effect on the model. The distances were median centered to avoid collinearity issues. p-Values presented are those associated with the coefficient of each term in the final model (in particular, they correspond to a test for difference from zero).

In addition, 95% confidence intervals on the predictions from (glmmPQL) mixture model M were estimated as follows: First, we calculated the model matrix X corresponding to predictions based on all possible combinations of independent variable levels

using the function model.matrix( ). Using X, we were able to estimate the variance of the predictions as

$$\text{diag}\,[X\% * \%\text{vcov}(M)\% * \%t(X)], \tag{2}$$

and used these, combined with the standard normal approximation to estimate the upper and lower confidence intervals as usual, i.e.,

$$\text{estimate} \pm Q \times \text{standard deviation (SD)},$$

where Q is the normal quartile corresponding to the required level of confidence and "tailedness" of the test, in this case $Q = 1.959964$ corresponding to a two-tailed test at the 95% confidence level. Regions in which the 95% confidence intervals of the two predicted curves being compared did not overlap were declared significantly different at the $p = 0.05$ level.

The measures listed below were analyzed by similarly constructing a glmmPQL model to predict the covariate value using the sole independent predictor of diet while retaining the mouse-specific random effect. The "family" was varied according to the data type of the dependent variable:

Total Dendritic Length: Gaussian
Branching points: Gaussian
Enclosing Radius: Poisson
Ramification Index fit: Gaussian, following log transform of dependent variable
Regression coefficient (Semi-log): Gaussian
Spine Density: Gaussian

Hippocampus Gene Expression Analysis

Female offspring from one TCDD-exposed litter and one control litter were culled at PND14 and hippocampi were dissected in ice-cold PBS and snap-frozen in liquid nitrogen. Samples were thawed into TRIzol Reagent solution (15596-018; Invitrogen) and RNA isolated using the Direct-zol RNA miniprep kit following the manufacturer's protocol (R2052; Zymo research). RNA concentration and purity were assessed using a NanoDrop spectrophotometer (Thermo Scientific) and TapeStation (Agilent). The mRNA library was prepared using the Poly A KAPA mRNA HyperPrep Kit (Kapa Biosystems Inc.) and single-end sequencing was performed on the Illumina HiSeq4000 platform.

FastQC (version 0.11.2) was used to check the quality of the raw sequencing data (http://www.bioinformatics.babraham.ac.uk/projects/fastqc), and then adaptor sequences were trimmed using Trim Galore! version 0.4.1 (http://www.bioinformatics.babraham.ac.uk/projects/trim_galore/). Reads were aligned to the mouse genome (GRCm38.p4) using TopHat (version 2.1.0), and featureCounts (version 1.5.0) was used to count reads aligned to genomic features (Kim et al. 2013; Liao et al. 2014). Differential expression testing was performed using DESeq2 (version 1.10.1) as previously described (Love et al. 2014), and an FDR cutoff threshold of 0.05 was used to filter for significantly differentially expressed genes. The R package ggplot2 (version 2.1.0) was used to generate volcano plots, and DESeq2 was used to generate normalized read count plots for individual genes. FDR <0.05 was used as threshold for significance for differentially regulated genes. Gene ontology (GO) and pathway analysis was performed in MetaCore™ (Clarivate Analytics) using Pathway maps, Process network, GO process, GO molecular, and Transcription factor interactions analyses. Default settings were used, including "intersection" as the distribution and "statistically significant" as the sorting method. The pathway maps and process network tools were used to generate figures visualizing the RNA sequencing results.

Validation by Quantitative-PCR (qPCR)

RNA samples were reverse transcribed using the nanoscript2 reverse transcription kit (RT-NanoScript2; PrimerDesign) and oligodT primers according to manufacturer's instructions. Quantitative PCR was carried out using the Luna® Universal qPCR Master Mix (M3003; New England Biolabs) in LightCycler 480 II (Roche), using the program recommended by the manufacturers: initial denaturation at 95°C for 60 s, 40 cycles of denaturation at 95°C for 15 s and extension at 60°C for 30 s, and a final melt curve step of 60°–95°C. Ct threshold values were normalized to the housekeeping gene *Gapdh* to calculate the ΔCt value. The ΔΔCt was then calculated relative to the control sample and relative expression calculated as $2^{-\Delta\Delta Ct}$. Sequences of qPCR primers (Integrated DNA Technologies, Inc.) used are shown in Table 2.

TCDD Analysis

Male offspring of dams exposed to the TCDD or control diet were culled at PND21 in a CO_2 chamber and the brains removed for analysis of TCDD concentration. Feed and mouse tissue were analyzed for PCDD/Fs as described by Lundebye et al. (2017). In brief, the analytes were extracted with hexane using an accelerated solvent extractor and purified by an automated PowerPrep system (FMS). PCDD/Fs were analyzed by high-resolution gas chromatography–high resolution mass spectrometry (HRGC-HRMS), with the concentration and the limit of quantification of TCDD reported (HRGC, Trace 2000 series; HRMS, DFS, Thermo Finnigan).

Results

To study the effects of a low-dose, persistent gestational exposure to TCDD, pregnant C57BL/6J mice were placed on the TCDD diet from the day of fertilization until PND2 (Figure 1). TCDD accumulation and persistence in the brains of offspring were confirmed by measuring TCDD levels in male pups at PND21 (Table 3).

No effects of TCDD exposure were detected on maternal weight gain during the pregnancy [$F(1,24) = 0.36$, $p = 0.55$], pup weight [females: $F(1,26) = 0.18$, $p = 0.67$, males: $F(1,25) = 1.4$, $p = 0.25$], litter size at birth [$t(25) = 0.059$, $p = 0.95$], the number of pups lost between birth and weaning [$t(25) = 0.63$, $p = 0.53$], or the sex ratio in each litter [$t(23) = 1.6$, $p = 0.13$] (Figure 2A–F).

Characterizing the Behavioral Effects of Gestational TCDD Exposure

Offspring of both sexes born to TCDD-exposed and control dams were tested in a battery of tests to investigate the behavioral outcomes of the exposure.

There was no significant diet effect on behavior in the open field test, suggesting that exposure to the TCDD diet did not affect anxiety-like behavior [females: $F(1,41) = 3.0$, $p = 0.09$, males: $F(1,46) = 0.80$, $p = 0.37$ Figure 2G,H; Figure S1A,B]. TCDD-exposed mice also displayed normal anxiety-like behaviors in the light-dark box and elevated plus maze tests (Figure S1C–F). Exposure to TCDD did not affect social and aggressive interactions with a novel conspecific in adult [females: $F(1,41) = 0.045$, $p = 0.83$, males: $F(1,46) = 0.39$, $p = 0.54$; Figure 2I,J] or juvenile mice (Figure S2A,B). Consistent with these findings, TCDD-exposed mice showed normal behaviors in the three-chamber social approach and social novelty test (Figure S2C–J). TCDD-exposed mice did not display significant differences from controls in repetitive behaviors in the self-grooming test [females: $F(1,39) = 0.060$, $p = 0.81$, males: $F(1,46) = 0.017$, $p = 0.90$; Figure 2K,L] or in the marble burying test (Figure S3a,b). Furthermore, ultrasonic vocalizations recorded following separation of pups from the mother did not reveal any significant effects of the TCDD diet on call

Table 2. Quantitative PCR primers for RNA sequencing validation.

Gene	Forward primer	Reverse primer
Eomes	ACAACTACGATTCATCCCATCAG	GGGCTTGAGGCAAAGTGTTG
Kif21b	GACTGCTGCGTCAAAGTGG	GGGTAACGGAGGTACAGATGT
Crmp5	GGTCTGCTGTGACTATGCCC	CTCCATTTCTGCTTTCACCTTGG
Tubb5	GCTGGACCGAATCTCTGTGT	CCCCAGACTGACCGAAAACG
Slc4a5	GGGTCAGGGAGCAGAGAGTTA	GGAAGACTCCATAGAGCACTGG
Sema3b	CACCTCCAGTGGTGTCTTCC	AAAGGTCCCAAGAAGGCTCG
Plxnb2	CTACTCTCCGTCAAGGGCAC	TGCCTGCTCGTCCAAGAAAT
Col8a1	GACGTGCTCAAGAAGCTGTTC	GAGGTGGCAGAGGCTTGATT
Gapdh	GCTCATGACCACAGTCCATGC	ATTGGGGGTAGGAACACGGA

Note: PCR, polymerase chain reaction.

Table 3. TCDD concentration in the diets and in brains of TCDD-exposed and control male offspring.

Diet	TCDD in diet (pg/g)	TCDD in PND21 brain (pg/g)
Control diet	<0.29	<LOQ (0.85 ± 0.07)
TCDD diet	45.5	5.73 ± 3.13

Note: Pregnant mice were fed the TCDD or control diet from the day the plug was found until 2 days after parturition. The brains of male offspring were flash-frozen at PND21 and analyzed for TCDD concentration, shown as mean ± SD. TCDD levels in all control diet brains analyzed were below LOQ (mean LOQ shown). $n = 3$ control pups from 2 litters and 3 TCDD-exposed pups from 3 litters. LOQ, the lowest concentration that can be reliably measured; SD, standard deviation; TCDD- 2,3,7,8 tetrachlorodibenzo-*p*-dioxin.

frequency [females: $F(1,29) = 1.16$, $p = 0.29$, males: $F(1,29) = 0.75$, $p = 0.39$; Figure 2M,N]. Adult mice were also tested for spatial novelty discrimination and did not display significant diet effects [females: $F(1,35) = 1.01$, $p = 0.32$, males: $F(1,46) = 0.40$, $p = 0.53$; Figure 2O,P].

The accelerating rotarod test was performed to investigate motor coordination and learning (Figure 3A,B). TCDD-exposed females fell off the rod faster than controls [$F(1,41) = 4.57$, $p = 0.039$], indicating a motor coordination deficit. There was no significant difference between the male diet groups [$F(1,46) = 1.00$, $p = 0.32$]. The deficit did not seem to be due to differences in muscle strength, because there were no significant differences between diet groups in the grip strength test (Figure 3C–F; *p*-values in Excel Table S1).

Spatial memory and learning were assessed using the MWM task. During the acquisition stage, diet had no significant effect on the time the mice took to reach the platform [females: $F(1,41) = 0.10$, $p = 0.76$, males: $F(1,46) = 0.01$, $p = 0.94$; Figure 4A,D]. There was no significant effect of diet on the time spent in each quadrant during a probe trial following the last day of acquisition [females: $F(1,41) = 1.16$, $p = 0.29$, males: $F(1,46) = 0.30$, $p = 0.59$; Figure 4B,E]. Both TCDD-exposed and control mice spent significantly more time in the quadrant that contained the platform than is expected by chance, suggesting all groups successfully learned the location of the platform [female controls: $t(22) = 7.438$, $p < 0.0001$, female TCDD: $t(21) = 8.840$, $p < 0.0001$, male controls: $t(16) = 4.60$, $p = 0.0003$, male TCDD: $t(32) = 6.06$, $p < 0.0001$]. There were no significant differences between the diet groups in swim speed or thigmotaxis, which could have confounded MWM results (Figure S4; Table S9).

During the reversal learning stage, TCDD exposure appeared to have a significant effect on females [$F(5,205) = 2.63$, $p = 0.025$; Figure 4C; ANOVA tables in Excel Table S2]. Although the female control group achieved significant reduction in path length over the reversal phase (day 1 vs. day 5 $p < 0.0001$), the TCDD-exposed females failed to achieve statistically significant reduction (day 1 vs. day 5 $p = 0.63$), suggesting increased behavioral inflexibility in TCDD-exposed females. There was no significant diet–time interaction for reversal learning in males [$F(4,184) = 1.05$, $p = 0.38$; Figure 4F].

The offspring were next tested in the hippocampus-dependent CFC test. The mice displayed no freezing behavior before the foot shocks, and there was no diet effect on freezing behavior after the first foot shock [females: $t(14) = 0.284$, $p = 0.78$, males: $t(14) = 0.785$, $p = 0.45$ Figure 4G,H]. When returned to the context 24 h later, TCDD-exposed males displayed almost twice as much freezing behavior as the control males (Figure 4J), suggesting that they have higher long-term contextual fear memory than controls had. However, this difference was not significant [$t(14) = 2.131$, $p = 0.051$; Figure 4J] and freezing behavior was generally low, as previously reported for C57BL/6J mice (Smith et al. 2007; Vigil et al. 2017).

In summary, low-dose repeated exposure to the TCDD diet during gestation led to differences in reversal learning and a motor coordination deficit in female offspring. These behavioral phenotypes were not confounded by differences in locomotor activity, muscle strength, or anxiety.

The Effects of Gestational TCDD Exposure on Brain Structure

Volumetric differences were assessed by structural MRI in 182 brain regions in absolute terms as well as relative to the total brain volume in adult mice of both sexes (Figure 5A). No significant differences were detected between the diet groups in the absolute volume of the whole brain and the absolute volumes of the 182 brain regions (Figure 5B; Excel Table S3). However, some differences in the size of several brain regions relative to the whole brain were observed (Figure 5C,D). The ventral region of the hippocampal formation appeared hyperplastic in the MRI heat maps, with the subiculum and the stratum lucidum regions larger in TCDD-exposed mice ($q = 0.079$ and $q = 0.043$, respectively). In the cerebellum, the interpositus nucleus was hyperplastic ($q = 0.079$), whereas the white matter around the hemispheric crus I was smaller in the TCDD group ($q = 0.074$). The mammillary bodies were also hypoplastic in the TCDD group ($q = 0.074$). As discussed in the "Methods" section, sex was covaried for in the linear model used to assess volumetric differences. Analyzing each sex separately revealed no statistically significant differences in relative or absolute volumes, most likely due to insufficient statistical power (Excel Table S4).

Sholl Analysis of Hippocampal CA1 Pyramidal Neurons in Juvenile and Adult Female Offspring

To investigate whether TCDD exposure affected hippocampal cell morphology, brains of PND21 and adult female offspring were stained with the Golgi Cox method to sparsely label individual cells. Female mice were used because behavioral phenotypes appeared more pronounced in females. Pyramidal neurons in the CA1 region of the hippocampus were imaged and traced (Figure 6A–C). Sholl analysis was used to assess dendritic morphology by drawing concentric circles around the center of the cell soma, and recording the number of intersections of a given circle with traced dendrites. The number of intersections was estimated with

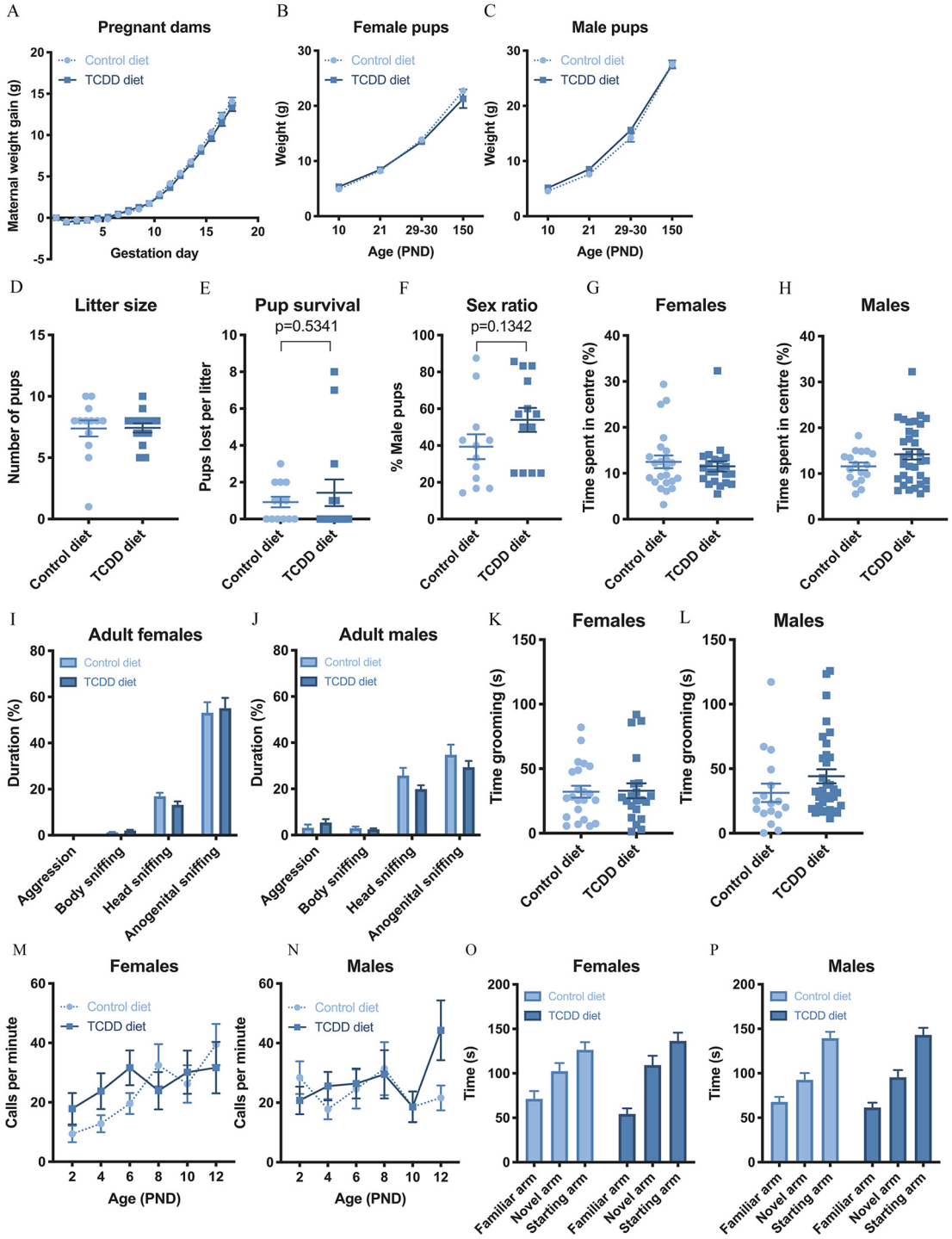

Figure 2. Weight, survival, anxiety-like behaviors, and ASD-like behaviors in mice exposed to TCDD during gestation. Pregnant C57BL/6J mice were fed the TCDD diet (9 ng TCDD/kg BW/day) or the control diet from E0.5 until the offspring were at PND2. Maternal weight gain over the course of the pregnancy (A), pup weight (B,C), litter size at birth (D), and the number of pups lost between birth and weaning (E) are shown for pups of both sexes. The sex ratio of the litters is shown (F). Adult offspring were tested in the open field test and the percentage of time spent in the center zone of the arena shown (G,H). Social behaviors adult mice were scored for 5 min during interaction with an unfamiliar sex-matched juvenile mouse. The percentage of time in which the test mouse was aggressive or sniffing the body, head and anogenital region of conspecific mouse is shown (I,J). Grooming behavior was scored from video over 10 min in an empty cage (K,L). Pups were separated from the mother and their ultrasonic vocalizations recorded over 3 min and manually quantified. Mean calls per minute on alternate PNDs 2-12 are shown (M,N). In the spontaneous spatial novelty discrimination test mice were allowed to explored two arms of the Y-maze for five minutes. An hour later, the mice were allowed to explore all three arms of the maze for 5 min, and the time spent in each of the arms of the Y-maze measured (o,p). Diet groups were compared using a three-way ANOVA (A–C,I,J,M–P), or a two-way ANOVA (D–H, K,L) with Sidak's multiple comparisons post hoc tests. Error bars are SEM. For (A), $n = 12$ control dams, 14 TCDD dams; for (B–C), $n = 13 - 15$ pups from $4 - 6$ litters; for (D–F), $n = 12 - 14$ TCDD litters. For (G–L,O,P) $n = 23$ control females, 22 TCDD females, 17 control males, 33 TCDD males from 8 litters per diet. For (M,N), $n = 17$ control females, 14 TCDD females, 17 control males, 14 TCDD males from 8 litters per diet. The numerical data corresponding to this figure are shown in Tables S1–S6. Note: ANOVA, analysis of variance; ASD, autism spectrum disorder; BW, body weight; E, embryonic day; PND, postnatal day; SEM, standard error of the mean; TCDD, 2,3,7,8 tetrachlorodibenzo-*p*-dioxin.

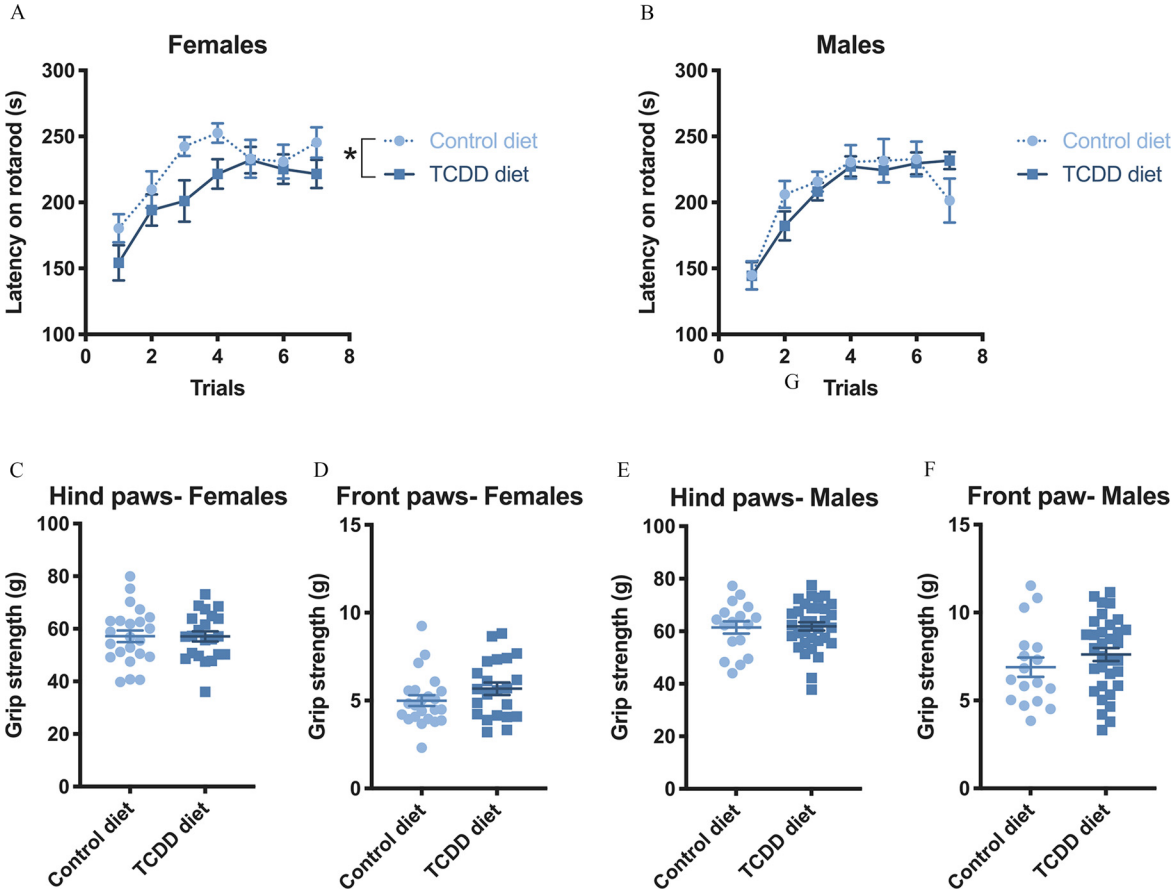

Figure 3. Motor coordination and grip strength in mice exposed to TCDD during gestation. Mice were tested on an accelerating rotarod seven times, with 5 min rest between trials (A,B). Grip strength of the hind paws and front paws of the mice were tested three times, and the average grip strength is shown (C–F). Diet groups were compared using a three-way ANOVA (A–B), or a two-way ANOVA (C–F) with Sidak's multiple comparisons post hoc tests. Error bars are SEM; $n = 23$ control females, 22 TCDD females, 17 control males, 33 TCDD males from 8 litters per diet. The numerical data corresponding to this figure are shown in Table S7. All p-values for (C–F) are shown in Excel Table S1. Note: ANOVA, analysis of variance; PND, postnatal day; SEM, standard error of the mean; TCDD, 2,3,7,8 tetrachlorodibenzo-p-dioxin. *Diet effect in ANOVA $p < 0.05$.

a generalized linear mixture model as described in the "Methods" section. [p-values shown in Table S12; for simplicity only p-values of the second term (c.distance^2:dietTCDD) are quoted in this section].

At PND21, pyramidal cells from TCDD-exposed female offspring had significantly more intersections than the control cells in the range of $70-145$ µm from the cell soma ($p = 0.0048$, Figure 7A; Excel Table S5). There was no significant difference between the diet groups in the basal arbor at PND21 ($p = 0.354$; Figure 7C). This increase in arborization was also present in adult females, where TCDD-exposed mice had significantly more apical dendritic intersections in the range of $15-130$ µm from the soma ($p = 1.24 \times 10^{-6}$; Figure 7B), and significantly more basal dendritic intersections in the range of $50-110$ µm from the soma ($p = 6.97 \times 10^{-7}$; Figure 7D).

Despite significant increases in arborization shown by the Sholl analysis, there were no significant differences in the total length of all dendrites (PND21: basal $p = 0.20$, apical $p = 0.22$, adult: basal $p = 0.09$, apical $p = 0.46$; Figure 7E) or the number of branching points (PND21: basal $p = 0.79$, apical $p = 0.46$, adult: basal $p = 0.84$, apical $p = 0.86$; Figure 7F). However, cells from TCDD-exposed adults had a significantly shorter enclosing radius ($p = 0.033$; Figure 7G), indicating a shorter apical length, and a significantly higher apical ramification index than controls indicated ($p = 0.0495$; Figure 7H). Adult TCDD-exposed mice also had a significantly higher apical regression coefficient than controls had ($p = 0.020$; Figure 7I), a measure of the rate of decay of the number of branches with distance from the soma.

To investigate the effect of the TCDD diet on dendritic spine formation, spines were manually counted along segments of apical and basal dendrites of at least 15 µm, excluding primary branches (Figure 7J). The diet had no significant effect on the dendritic spine density in adult CA1 pyramidal neurons (basal $p = 0.34$, apical $p = 0.61$).

Gene Expression in the Hippocampus of TCDD-Exposed Female Offspring

To determine whether these differences in neuronal morphology were associated with abnormal gene expression during the postnatal period when pyramidal cells are in the process of extending and developing their dendritic arbor (Pokorný and Yamamoto 1981), we used RNA sequencing to compare gene expression in the hippocampi of female PND14 TCDD-exposed and control offspring.

This analysis identified 405 differentially expressed genes (FDR <0.05), with principal component analysis indicating clear separation between control and TCDD samples (Figure 8A,B; genes listed in Excel Table S6). Only 36 genes were up-regulated in the TCDD-exposed group, with 369 (91%) down-regulated. To validate these differences, the expression of eight differentially expressed genes was analyzed by qPCR (Figure 8C,D). Four of the eight genes tested showed significant differences as expected

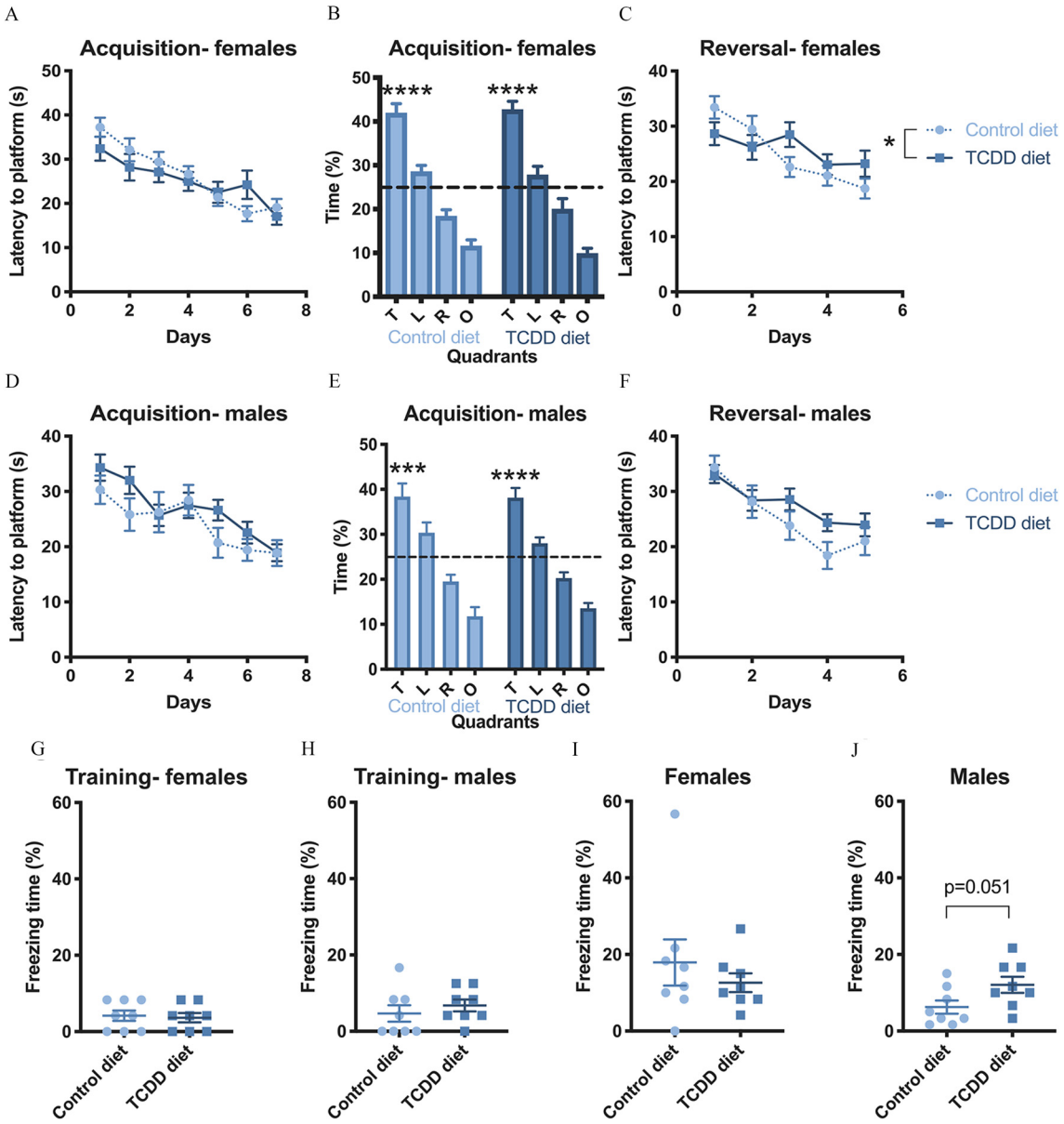

Figure 4. Hippocampus-dependent learning tests in mice exposed to TCDD during gestation. Adult TCDD-exposed or control offspring were tested in the Morris water maze (MWM) task. After 7 d in the "acquisition" stage of the task, the platform was moved to the opposite side of the maze, and the mice were tested for reversal learning during the "reversal" stage. The average length of the path taken to the platform over four trials per day is shown for the acquisition stage (A,D) and for the reversal stage (C,F). A probe trial was carried out on the last day of acquisition (B,E). The time spent in each quadrant of the maze is shown, with the dotted line indicating the amount of time expected by chance (25%). Mice were trained for contextual fear conditioning, and freezing rates were scored during the training following the first foot shock (G,H) and 24 h later in the conditioned environment (I,J). Diet groups were compared using a three-way ANOVA with Sidak's multiple comparisons post hoc tests (A–F), a two-way ANOVA with Sidak's multiple comparisons post hoc tests (G–H) or an unpaired Student *t*-test (I,J). For (B,E), a one-sample Student *t*-test was used to determine whether the mice spent more than 25% of the time in the target quadrant. Error bars are SEM; for (A–F) $n=23$ control females, 22 TCDD females, 17 control males, 33 TCDD males from 8 litters per diet. For (G–J) $n=8$ females and 8 males per diet from 4 – 6 litters per diet. Quadrants: target (T) (containing the platform), opposite (O), right (R), left (L). The numerical data corresponding to this figure is shown in Table S8. All *p*-values for (C,F) are shown in Excel Table S2. Note: ANOVA, analysis of variance; MWM, Morris water maze; SEM, standard error of the mean; TCDD, 2,3,7,8 tetrachlorodibenzo-*p*-dioxin. $^{*}p<0.05$, $^{**}p<0.01$, $^{***}p<0.001$, $^{****}p<0.0001$.

from the RNA sequencing data [*Eomes* $t(5)=3.93$, $p=0.011$, *Crmp3* $t(5)=2.76$, $p=0.040$, *Slc4a5* $t(5)=4.41$, $p=0.0070$, and *Col8a1* $t(5)=4.86$, $p=0.0046$]. Another two of the genes tested showed the expected trend but did not reach statistical significance [*Tubb5* $t(5)=1.945$, $p=0.1094$, *Sema3b* $t(5)=1.059$, $p=0.3381$]. Finally, two of the genes tested did not show the differences in expression expected [*Kif21b* $t(5)=0.31$, $p=0.77$ and *Plxnb2* $t(5)=0.12$, $p=0.91$], possibly because they displayed relatively small expression differences in the RNA sequencing (log-FoldChange = 0.27 and −0.27, respectively).

Differentially expressed genes were analyzed using enrichment analysis in MetaCore™ (Excel Tables S7–S15). MetaCore™ provides pathway maps and networks of interactions between genes and proteins curated from the literature. The up-regulated gene list was enriched for processes and pathways involving the cytoskeleton, cell adhesion, axon guidance, and neurogenesis (Table 4). The "axonal guidance" process network was enriched with the lowest FDR (1.01×10^{-5}), with gestational TCDD exposure leading to up-regulation of tubulins (*Tubb5*, *Tubb2b*, *Tuba1a*, and *Tubb3*), CRMP genes (*Crmp1*, *Crmp3*, *Crmp5*),

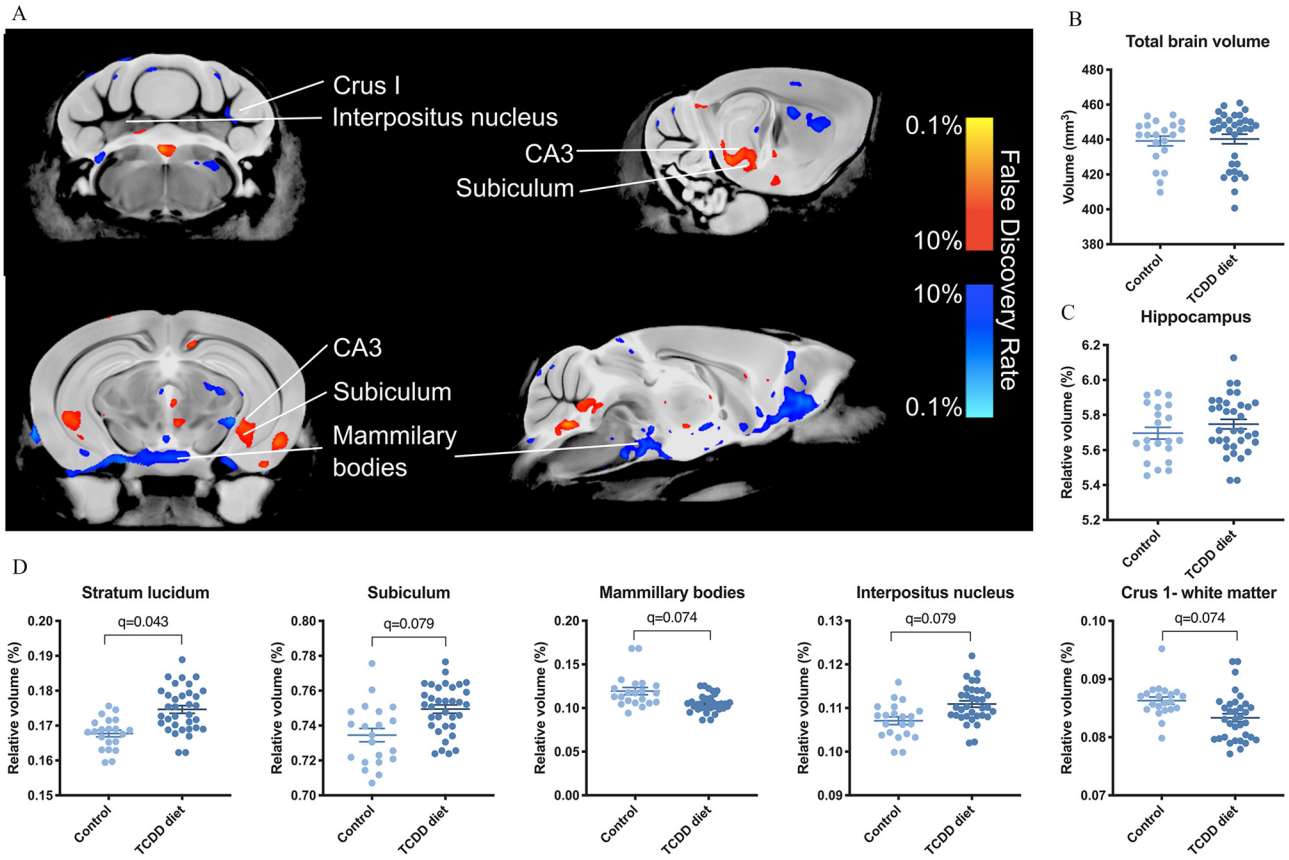

Figure 5. Panel A shows voxel-wise comparisons of high-resolution 7T structural MRI images of brains of control and TCDD-exposed adult mice; areas that were larger in TCDD-exposed mice are shown in red-yellow, and areas that were smaller are shown in dark-light blue. The absolute total brain volume of each mouse is shown (B), as well as the volumes of brain regions relative to the total brain size (%) (C,D). Multiple comparisons were controlled for using the false discovery rate; significance is based on covarying for total brain volume and sex. Error bars are SEM; $n = 21$ Controls and 34 TCDD brains from 8 litters per diet. The numerical data corresponding to this figure are shown in Table S10 and in Excel Table S3. Note: MRI, magnetic resonance imaging; SEM, standard error of the mean; TCDD, 2,3,7,8 tetrachlorodibenzo-*p*-dioxin.

Doublecortin (*Dcx*), and Ephrin type B receptor 2 (*Ephb2*), and down-regulation of Semaphorin 3b (*Sema3b*) and Plexin B2 (*Plxnb2*). The top most-enriched pathway maps were "cytoskeleton remodelling_ neurofilaments" (FDR $= 2.92 \times 10^{-5}$ pathway shown in Figure S5, Figure S7) and "Regulation of cytoskeleton proteins in oligodendrocyte differentiation and myelination" (FDR $= 2.92 \times 10^{-5}$; Table 4). GO process analysis indicated enrichment of genes involved in axon and dendrite guidance, cytoskeleton regulation, synapse organization, and in neurogenesis (Excel Table S8).

Gene ontology analysis for enrichment of down-regulated genes revealed enrichment of genes in pathways involving extracellular matrix (ECM) interactions and remodeling, and in cell adhesion, with the pathway map enriched with the lowest FDR being "Role of cell-cell and ECM-cell interactions in oligodendrocyte differentiation and myelination," (FDR $= 1.88 \times 10^{-5}$, Table 5; pathway shown in Figure S6, S7). Several enriched pathways concerned oligodendrocytes, myelination, and/or multiple sclerosis, with down-regulated genes including Myelin basic protein (*Mbp*) and Myelin associated glycoprotein (*Mag*). The other major component of the myelin sheath, Proteolipid-protein (*Plp1*), also displayed a trend for lower expression in the TCDD-exposed offspring, but the difference did not quite reach statistical significance (FDR $= 0.076$). Analysis for enrichment of genes in process networks also pointed toward networks involving ECM and cell adhesion. Ten collagen genes were down-regulated in the TCDD data set, as well as genes involved in ECM regulation, such as Matrix Metalloproteinase-2 (*Mmp2*), and Tissue Inhibitor of MetalloProteinase 3 (*Timp3*).

To identify the transcription factors most likely responsible for the altered gene expression, we used MetaCore™ transcription factor analysis (Table 6; Excel Table S15). The TCDD-receptor, AHR was significantly enriched ($p = 0.002724$, z-score $= 3.375$). The most enriched transcription factor was the TGFβ intercellular signaling transducer, SMAD3 ($p = 8.209 \times 10^{-17}$, z-score $= 11.8$). In the MetaCore™ database, SMAD3 was identified as a transcriptional regulator of 36 of the genes in the data set, with three of these being up-regulated (*Eomes*, *Cdk5r1*, and *Tnc*) and 33 down-regulated. These genes included TGFβ pathway genes (*Tgfbi* and *Tgfbr3*) and ECM remodeling genes (*Mmp2*, *Timp3*, four collagen genes). In summary, gene expression analysis indicates dysregulation of the TGFβ-SMAD3 pathway, extracellular matrix, and microtubules in the hippocampus of TCDD-exposed mice.

Discussion

In this study, a continuous exposure of pregnant mice to low levels of TCDD in the diet was found to have subtle effects on reversal learning and motor coordination in female offspring. Small differences between diet groups in the relative volumes of brain regions in the hippocampal formation, cerebellum, and mammillary bodies were observed. The expression of more than 400 genes was significantly altered in the PND14 hippocampus, and higher arborization of CA1 pyramidal neurons was observed in PND21 and adult TCDD-

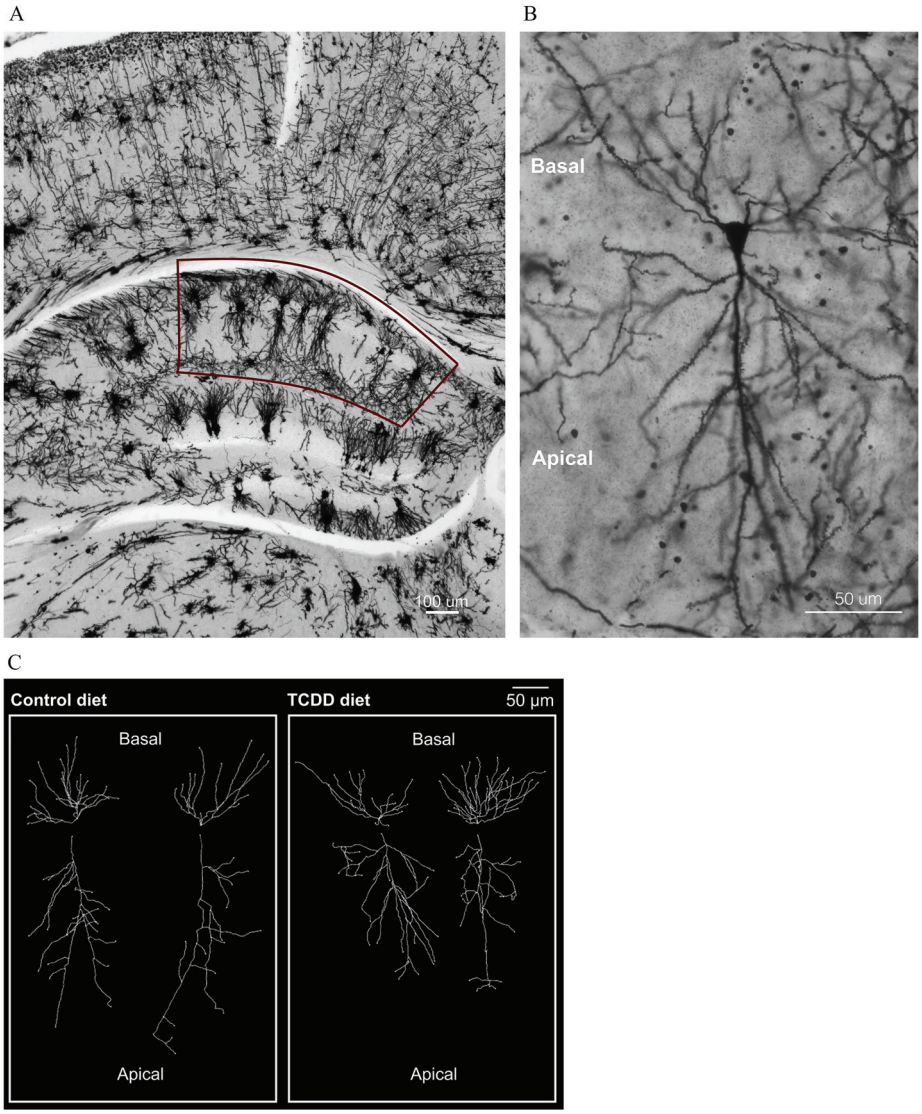

Figure 6. Golgi labeling of hippocampal pyramidal neurons in female mice exposed to TCDD during gestation. (A) A representative image of Golgi stained coronal section showing the dorsal hippocampus of a PND21 female control mouse. Pyramidal cells from the CA1 region (circled in red) were imaged for morphological analysis. (B) shows a high-power image of a CA1 neuron used for morphological analysis. (C) displays representative examples of traces of the neurons showing two cells from TCDD-exposed and two cells from control diet–exposed. Note: CA, Cornus Ammonis; PND, postnatal day; TCDD- 2,3,7,8 tetrachlorodibenzo-*p*-dioxin.

exposed female offspring. These findings show that exposure of a pregnant dam to 9 ng TCDD/kg BW/d during gestation is sufficient to cause specific changes in neuronal structure, brain anatomy, gene expression, and learning and motor behaviors in female offspring.

A Model of Dietary TCDD Exposure during Gestation

Animal studies of gestational TCDD exposure have generally used single exposure protocols resulting in body burdens far above LOAEL (EFSA CONTAM Panel 2018). In our exposure protocol, pregnant mice were exposed to a daily dose of 9 ng/kg BW, with a cumulative dose of around 200 ng/kg BW. To our knowledge this is the first rodent study to identify abnormal behavior, gene expression, and neuronal morphology in mice exposed to less than 100 ng TCDD/kg BW/d throughout gestation.

At PND21, the average TCDD concentration in the offspring brains was 5.73 pg/g, about half the concentration found in the brains of PND14 mice exposed to 600 ng TCDD/kg BW at E12.5 (Kimura et al. 2015). Comparable measurements in human brains are not available, but similar concentrations of TCDD in breast milk have been associated with neurodevelopmental phenotypes in children (Nishijo et al. 2014; Pham et al. 2015). Measurements of TCDD and related congeners identified mean concentration of 1.4 – 5.3 pg TEQ/g fat in livestock meat for human consumption (EFSA CONTAM Panel 2018). Taking into account the fact that the half-life of TCDD is much shorter in rodents than in humans (Pirkle et al. 1989; Emond et al. 2006), the TCDD exposure of <10 ng/kg BW/d used in our study seems highly relevant in an attempt to model the neurodevelopmental consequences of environmental TCDD exposure during pregnancy.

Learning and Motor Behavioral Outcomes of Gestational Low-Dose TCDD Exposure

Although subtle, the differences in reversal learning in the MWM observed in the present study could point toward changes in cognitive inflexibility, an ASD-like behavior (Crawley 2004), or to effects on spatial and visual memory (Vorhees and Williams 2014). The TCDD exposure regime did not affect swim speed or performance during the acquisition stage of the test, indicating

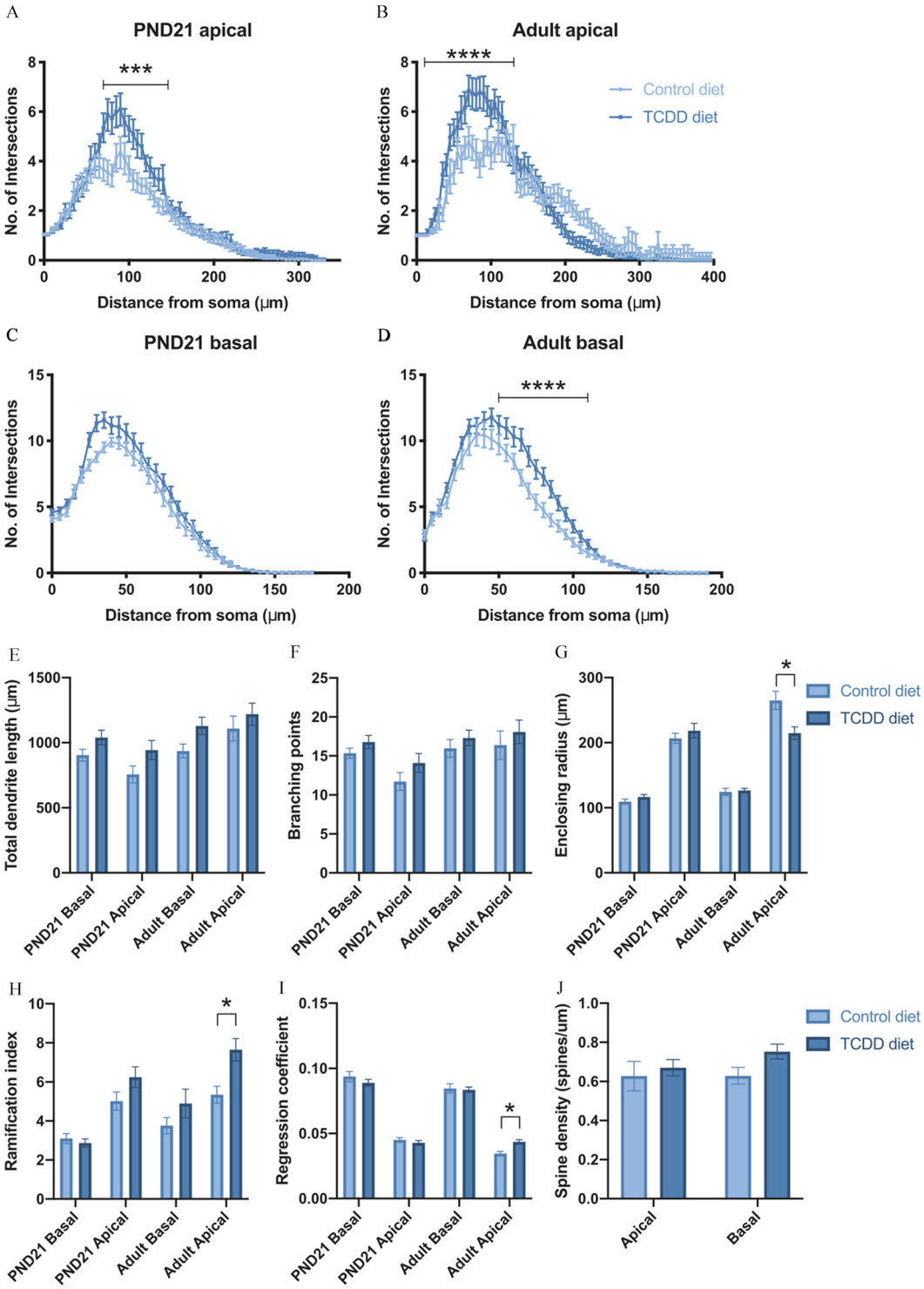

Figure 7. Morphology of CA1 pyramidal neurons of PND21 and adult female mice exposed to TCDD during gestation. The brains of TCDD-exposed and control females were sectioned coronally and Golgi stained. CA1 pyramidal neurons were imaged, and their dendrites were traced. Sholl analysis was carried out as shown for PND21 apical (A) and basal (C) and adult apical (B) and basal (D) dendritic branches. The range of distances from the soma where there was a significant difference between the diet groups is indicated. (E) shows total length of all of the dendrites traced. (F) Number of branching points in the arbor. (G) displays the enclosing radius, the furthest radius at which there was an intersection between the Sholl circles and a dendritic branch. (H) shows Schoenen ramification index, the ratio between the local maximum of the polynomial fit of the data, and the number of primary branches. (I) shows the Sholl regression coefficient calculated using a semi-log linear regression of the Sholl data. (J) Spines were manually counted along segments of apical and basal dendrites of at least 15 μm, excluding primary branches. The effects of the diet on the CA1 morphology were assessed using glmmPQL models as described in the methods. For (A–D), all sample sizes and p-values shown in Table S12; for simplicity only p-values of the second term (c.distance^2:dietTCDD) are shown in this figure. For (A–I), $n = 11 - 39$ dendrites from 3–4 mice of each diet, each from a different litter. For (J), $n = 13 - 36$ cells from 3–4 mice, each from a different litter. The numerical data corresponding to this figure is shown in Table S11 and in Excel Table S5. Note: CA, Cornu Ammonis; PND, postnatal day; TCDD, 2,3,7,8 tetrachlorodibenzo-p-dioxin. $^{*}p < 0.05$, $^{**}p < 0.01$, $^{***}p < 0.001$, $^{****}p < 0.0001$.

that the reversal learning phenotype was not a result of motor defects. Gestational TCDD exposure also leads to deficits in reversal learning in rhesus monkeys and rats (Schantz and Bowman 1989; Schantz et al. 1996; Seo et al. 1999), suggesting that cognitive inflexibility as a consequence of TCDD exposure is not restricted to rodents and might therefore be relevant to humans. The motor coordination deficit observed in the present study is in agreement with previous TCDD exposure studies that identified motor development deficits in rats and humans (Nishijo et al. 2007, 2012; Tai et al. 2016; Tran et al. 2016; Pham et al. 2019).

Sexually dimorphic effects on behavior have been observed in many of the TCDD exposure studies, with several pointing to greater disruption of learning or cognitive development in males than in females (Seo et al. 1999; Mitsui et al. 2006; Kishi et al. 2013; Tran et al. 2016). TCDD-exposed rats performed better in a visual learning task, with males exhibiting enhanced performance at the initial learning stage, and females performing better at a reversal learning stage (Widholm et al. 2003). This pattern, consistent with our findings, could suggest that males are more susceptible to TCDD effects on memory and learning, whereas females are more sensitive to effects on reversal learning and behavioral flexibility. Overall, the behavioral phenotypes identified in this study were subtle, suggesting the exposure dose might be near the LOAEL for behavioral effects.

Brain Morphology Outcomes of Gestational Low-Dose TCDD Exposure

Gestational TCDD exposure did not significantly affect the size of the brain or different brain regions but appeared to have a marginal effect on the relative size of regions of the cerebellum and hippocampal formation. These effects may relate to the motor coordination and behavioral abnormalities in the MWM, respectively. These findings suggest a particular vulnerability of these brain regions, and one might expect exacerbated phenotypes in these regions on exposure to higher doses.

The cerebellum plays a key role in motor coordination and learning (Ito 2000). Developmental roles for AHR in the cerebellum have been identified, and TCDD exposure can disrupt cerebellum development (Collins et al. 2008; Dever et al. 2016; Sarić et al. 2020). An interesting finding is that mice with a deletion of *Ahr* in cerebellum neural progenitors performed better than controls in the rotarod test (Dever 2013), consistent with our observation of motor deficits in TCDD-exposed mice.

Effects on the relative volumes of the mammillary bodies, subiculum, and stratum lucidum, areas with important roles in learning and memory (Morris et al. 1990; Galani et al. 1997; Hildebrandt et al. 2001; Vann and Aggleton 2003; Potvin et al. 2009; Aggleton and Christiansen 2015) were observed. The ventral subiculum is thought to be important for emotion and motivated behaviors, with lesions in the ventral subiculum leading to fear conditioning deficits (O'Mara, 2006; Maren et al. 2013). The stratum lucidum layer contains the mossy fibers, axonal projection from the granule cells of the dentate gyrus (DG) to neurons in the hilar and CA3 regions (McBain 2008).

We found that CA1 neurons in adult TCDD-exposed brains displayed shorter apical length and an increase in arborization in the proximal, but not distal, apical domain. As the proximal dendrites receive input from the CA3 region, one might predict that the very critical relay of information from CA3 to CA1 might be disrupted in TCDD-exposed brains (Spruston 2008; Jonas and Lisman 2014). Kimura et al. previously reported that a single dose of TCDD (600 or 3,000 ng/kg BW by gavage on E12.5) affected apical branch length of CA1 pyramidal neurons at PND14 (Kimura et al. 2015). It is difficult to directly compare the observed changes with the Kimura study, because they did not carry out a Sholl analysis, and so the overall effect on arborization is unclear. Kimura et al. did not detect the branching phenotype in aged mice, which suggested the phenotype was transient. Kimura et al. also identified a decrease in dendritic spine density on the CA1 neurons of aged mice, a phenotype we did not observe in adult mice (Kimura et al. 2015). These differences could indicate age-related, dose-dependent effects of TCDD exposure.

Granule cells of the dentate gyrus in $Ahr^{-/-}$ mice show a similar morphological phenotype to the phenotype we observed in TCDD-exposed mice, namely higher arborization in proximal apical dendrites and a shorter apical length (de la Parra et al. 2018). This similarity could suggest that TCDD exposure disrupts the physiological role of AHR, resulting in similar phenotypes in loss of AHR and TCDD exposure models. This principle has been observed in other neurodevelopmental contexts, for example both germline deletion of *Ahr* and exposure to a TCDD dose reduce proliferation, differentiation, and survival of neural stem cells in the adult DG (Latchney et al. 2013).

Transcriptional Outcomes of Gestational Low-Dose TCDD Exposure

Although our analysis suggested a significant enrichment of AHR targets among the dysregulated genes, classical AHR targets such as *Cyp1a1* were not up-regulated in the hippocampus of TCDD-exposed offspring, consistent with other studies that also found no evidence for *Cyp* gene induction in the brain by TCDD exposure (Unkila et al. 1993; Rasinger et al. 2014). It appears that the majority of genes dysregulated are not direct AHR targets but regulated by factors downstream of AHR.

Our data suggested that TCDD exposure during gestation led to the altered expression of genes regulated by SMAD3, providing further evidence for significant interactions previously identified between the AHR and TGFβ-SMAD3 pathways, both during normal development and disease contexts (Gramatzki et al. 2009; Cheng et al. 2020; Nakano et al. 2020; Sarić et al. 2020). Most of the 36 SMAD3 targets identified in our data set were down-regulated in the TCDD-exposed hippocampi, suggesting that TGFβ signaling may be down-regulated by TCDD exposure. Various mechanisms have been suggested for the regulation of TGFβ signaling by AHR, including transcriptional regulation of the TGFβ ligands, mediation of inhibition by integrins, repression of Latent Transforming growth factor β Binding Protein (LTBP1) expression, and inhibition of SMAD3 activation (Zaher et al. 1998; Chang et al. 2007; Peng et al. 2008; Gomez-Duran et al. 2009; Silginer et al. 2016; Sarić et al. 2020). TGFβ signaling is thought to play various roles in the central nervous system, including regulation of dendritic growth (Yu et al. 2014), neural survival and differentiation (Flanders et al. 1991; Kandasamy et al. 2014), and axon specification (Yi et al. 2010).

The up-regulated gene list was enriched for genes involved in neurogenesis and neuronal differentiation. A single dose of TCDD (20 ng/kg BW administered by gavage at E8.5) and germline deletion of *Ahr* have been previously shown to disrupt the development of neural progenitors in the DG (Latchney et al. 2013; Kobayashi et al. 2015). It remains to be seen if the up-regulation of *Dcx* and *Eomes* in the postnatal hippocampus disrupts the proliferation and differentiation of neuronal progenitors in the TCDD-exposed hippocampus.

GO analysis also pointed toward dysregulation of myelination and oligodendrocyte function in the TCDD-exposed brains. AHR signaling has a role in oligodendrocyte differentiation and function, with $Ahr^{-/-}$ mice displaying significant defects in the optic nerve myelin sheath (Juricek et al. 2017). A single oral dose of 700 ng/kg BW TCDD at E18 inhibited oligodendrocyte

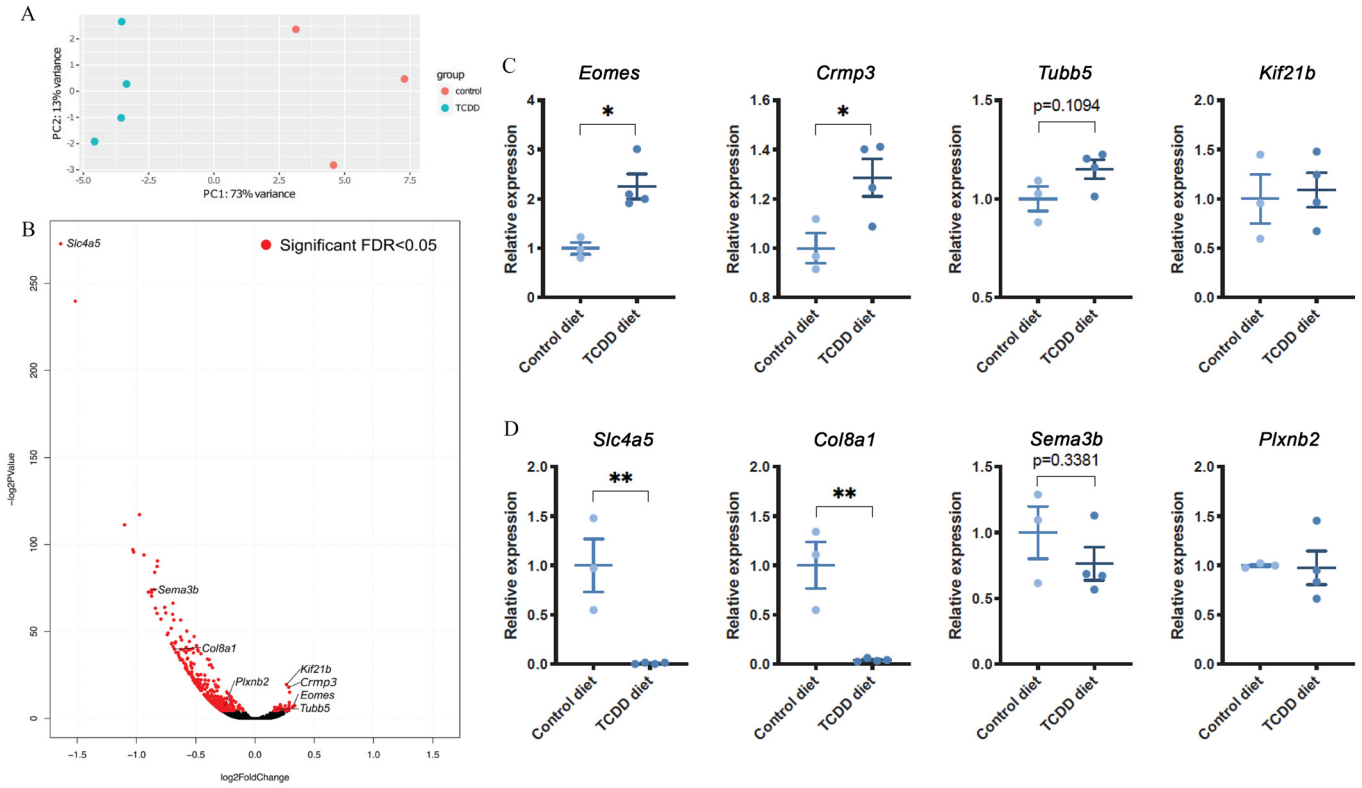

Figure 8. RNA sequencing of hippocampus samples from PND14 female TCDD-exposed and control offspring. cDNA libraries were made from whole hippocampi and sequenced as described in the "Methods" section. Significantly differentially expressed genes were identified with DESeq2 using an FDR threshold of 0.05. (A) Principal component analysis plot generated using the plotPCA function in DESeq2. (B) Volcano plot indicating differentially expressed genes in hippocampi from TCDD-exposed offspring compared to control. Each point represents an individual gene, and all significantly differentially expressed genes (FDR <0.05) are highlighted in red. The expression of eight of the differentially expressed genes was measured using quantitative PCR in hippocampus samples from PND14 female offspring. Expression normalized to Gapdh expression and to average expression of the control samples. (C) Genes up-regulated in the RNA sequencing data set. (D) Genes down-regulated in the RNA sequencing data set. For (C–D), diet groups compared using the Student *t*-test. Note: FDR, false discovery rate; PND, postnatal day; TCDD, 2,3,7,8 tetrachlorodibenzo-*p*-dioxin. $^{*}p < 0.05$, $^{**}p < 0.01$, $n = 3$ Control and 4 TCDD mice from 1 litter each.

Table 4. Significantly enriched pathways and process networks in the up-regulated gene list of TCDD-exposed hippocampus samples.

#	Pathway maps	*p*-Value	FDR
1	Development_Regulation of cytoskeleton proteins in oligodendrocyte differentiation and myelination	1.488×10^{-7}	2.923×10^{-5}
2	Cytoskeleton remodeling_Neurofilaments	2.302×10^{-7}	2.923×10^{-5}
3	Cell adhesion_Gap junctions	4.949×10^{-7}	4.190×10^{-5}
4	Tau pathology in Alzheimer disease	5.932×10^{-6}	3.767×10^{-4}
5	Stem cells_Schema: Adult neurogenesis in the Subventricular Zone	9.083×10^{-6}	4.614×10^{-4}
6	Inhibition of Ephrin receptors in colorectal cancer	3.745×10^{-5}	1.448×10^{-3}
7	Cytoskeleton remodeling_Reverse signaling by Ephrin-B	4.562×10^{-5}	1.448×10^{-3}
8	Cell cycle_Role of Nek in cell cycle regulation	4.562×10^{-5}	1.448×10^{-3}
9	Cytoskeleton remodeling_Keratin filaments	6.528×10^{-5}	1.842×10^{-3}
10	Inhibition of remyelination in multiple sclerosis: regulation of cytoskeleton proteins	1.197×10^{-4}	3.040×10^{-3}
#	Process networks	*p*-Value	FDR
1	Development_Neurogenesis_Axonal guidance	1.872×10^{-7}	1.011×10^{-5}
2	Cytoskeleton_Regulation of cytoskeleton rearrangement	4.429×10^{-7}	1.196×10^{-5}
3	Cell adhesion_Integrin-mediated cell-matrix adhesion	1.458×10^{-6}	2.625×10^{-5}
4	Cytoskeleton_Spindle microtubules	4.006×10^{-6}	5.408×10^{-5}
5	Cytoskeleton_Cytoplasmic microtubules	5.473×10^{-6}	5.911×10^{-5}
6	Cytoskeleton_Intermediate filaments	2.977×10^{-4}	2.679×10^{-3}
7	Cell adhesion_Attractive and repulsive receptors	6.239×10^{-4}	4.668×10^{-3}
8	Cell cycle_Mitosis	6.916×10^{-4}	4.668×10^{-3}
9	Cell adhesion_Glycoconjugates	3.939×10^{-3}	2.127×10^{-2}
10	Cell adhesion_Cell junctions	3.939×10^{-3}	2.127×10^{-2}

Note: RNA sequencing was carried out on whole hippocampus samples from TCDD-exposed and control female offspring at PND14. Enrichment analysis for pathway maps, process networks, GO processes, and GO molecular functions was carried out using MetaCore™ (Clarivate Analytics), with the full results shown in Excel Tables S7–S15. Pathway maps and process networks for the up-regulated gene list were ranked by FDR and the top 10 are shown here. FDR, false discovery rate; GO, gene ontology; PND, postnatal day; TCDD, 2,3,7,8 tetrachlorodibenzo-*p*-dioxin.

Table 5. Significantly enriched pathways and process networks in the down-regulated gene list of TCDD-exposed hippocampus samples.

#	Pathway maps	*p*-Value	FDR
1	Development_Role of cell-cell and ECM-cell interactions in oligodendrocyte differentiation and myelination	2.094×10^{-9}	1.876×10^{-6}
2	Inhibition of remyelination in multiple sclerosis: role of cell-cell and ECM-cell interactions	4.548×10^{-8}	2.037×10^{-5}
3	Stem cells_Role of TGF-beta 1 in fibrosis development after myocardial infarction	1.982×10^{-6}	4.255×10^{-4}
4	Cell adhesion_ECM remodeling	2.356×10^{-6}	4.255×10^{-4}
5	Stem cells_Hypothetical role of microRNAs in fibrosis development after myocardial infarction	2.720×10^{-6}	4.255×10^{-4}
6	IL-1 beta- and Endothelin-1-induced fibroblast/ myofibroblast migration and extracellular matrix production in asthmatic airways	2.849×10^{-6}	4.255×10^{-4}
7	Canonical WNT signaling pathway in colorectal cancer	9.565×10^{-6}	1.224×10^{-3}
8	Extracellular matrix-regulated proliferation of airway smooth muscle cells in asthma	1.702×10^{-5}	1.906×10^{-3}
9	Role of thyroid hormone in regulation of oligodendrocyte differentiation in multiple sclerosis	2.533×10^{-5}	2.522×10^{-3}
10	FGF2 signaling in melanoma	3.243×10^{-5}	2.906×10^{-3}
#	Process networks	*p*-Value	FDR
1	Cell adhesion_Cell-matrix interactions	1.077×10^{-14}	1.498×10^{-12}
2	Proteolysis_ECM remodeling	5.121×10^{-7}	3.559×10^{-5}
3	Development_Ossification and bone remodeling	6.570×10^{-6}	3.044×10^{-4}
4	Development_Cartilage development	1.200×10^{-5}	4.172×10^{-4}
5	Cell adhesion_Integrin-mediated cell-matrix adhesion	8.789×10^{-5}	2.443×10^{-3}
6	Proteolysis_Connective tissue degradation	1.074×10^{-4}	2.488×10^{-3}
7	Cell adhesion_Platelet-endothelium-leucocyte interactions	3.275×10^{-4}	6.504×10^{-3}
8	Development_EMT_Regulation of epithelial-to-mesenchymal transition	4.781×10^{-4}	8.306×10^{-3}
9	Cell adhesion_Cell junctions	1.791×10^{-3}	2.766×10^{-2}
10	Cell adhesion_Amyloid proteins	2.984×10^{-3}	4.148×10^{-2}

Note: RNA sequencing was carried out on whole hippocampus samples from TCDD-exposed and control female offspring at PND14. Enrichment analysis for pathway maps, process networks, GO processes, and GO molecular functions was carried out using MetaCore™ (Clarivate Analytics), with the full results shown in Excel Tables S7–S15. Pathway maps and process networks for the down-regulated gene list were ranked by FDR and the top 10 are shown here. ECM, extracellular matrix; EMT, epithelial-to-mesenchymal transition; FDR, false discovery rate; GO, gene ontology; PND, postnatal day; TCDD, 2,3,7,8 tetrachlorodibenzo-*p*-dioxin; TGF, transforming growth factor.

differentiation in rat offspring (Fernández et al. 2010), and the down-regulation of myelination related genes (*Mbp*, *Mag*) in the present study is consistent with TCDD exposure inhibiting the differentiation of oligodendrocytes or reducing their numbers in the hippocampus.

Our gene expression data suggest a potential mechanism for the abnormal dendritic structure of hippocampal neurons in TCDD-exposed mice. In addition to several tubulin genes, four of the five *Crmp* genes were up-regulated in TCDD-exposed hippocampi. CRMP proteins can positively and negatively regulate microtubule polymerization dynamics through interaction with tubulins, allowing them to regulate neurite outgrowth (Fukata et al. 2002; Uchida et al. 2005; Yoshimura et al. 2005; Aylsworth et al. 2009; Brot et al. 2010; Takaya et al. 2017; Ji et al. 2018). In addition, many of the genes involved in the axon guidance have been described to have vital roles in regulation of dendritic arborization (Ledda and Paratcha 2017). TCDD exposure also led to down-regulation of *Mmp2* and *Timp3*, genes involved in ECM proteolysis. *Mmp2* has been linked to demyelination, axonal outgrowth after injury, regulation of neurogenesis, and dendritic morphology (Duong and Erickson 2004; Ayoub et al. 2005; Gonthier et al. 2009; Verslegers et al. 2013, 2015). As several CRMP proteins are regulated by MMP2 (Verslegers et al. 2015). It is therefore possible that *Crmp* genes are up-regulated in the TCDD-exposed hippocampi to compensate for down-regulation of *Mmp2*.

Together, these findings allow us to propose a model of how TCDD exposure might lead to altered dendritic morphology in the hippocampus (Figure 9). In this model, TCDD activation of the AHR pathway represses the TGFβ-SMAD3 pathway, resulting in the down-regulation of ECM genes and *Mmp2*. The down-regulation of *Mmp2* leads to the up-regulation of *Crmp* genes, driving increased microtubule stability and/or growth resulting in increased dendritic arborization. Future studies will be needed to test this model. It would also be important to confirm our findings in independent studies, given the limitations of small sample size

Table 6. Transcription factor interactions analysis in MetaCore™ (Clarivate Analytics).

Network object name	Interacting genes in gene list	Expected	Ratio	*p*-Value	*z*-Score
SMAD3	36	6.474	5.561	8.209×10^{-17}	11.8
SP1	88	31.95	2.755	1.94×10^{-18}	10.39
Scleraxis	3	0.09249	32.44	0.00006115	9.651
TAL1	251	165.7	1.515	9.541×10^{-17}	8.446
SP3	36	9.97	3.611	3.714×10^{-11}	8.416
NFIC	9	0.9619	9.357	4.253×10^{-7}	8.281
c-Jun	50	17.07	2.929	1.172×10^{-11}	8.202
GCNF	8	0.7954	10.06	1.058×10^{-6}	8.161
SOX5	9	1.036	8.688	8.204×10^{-7}	7.907
C11orf9	6	0.4994	12.01	8.245×10^{-6}	7.861

Note: RNA sequencing was carried out on whole hippocampus samples from TCDD-exposed and control female offspring at PND14. Top ten most enriched transcription factors as ranked by *z*-score are shown. Ratio = number of interacting genes/expected number of interacting genes. *z*-Scores = (Ratio)/(square root of variance). The full list is shown in Excel Table S15. PND, postnatal day; TCDD, 2,3,7,8 tetrachlorodibenzo-*p*-dioxin.

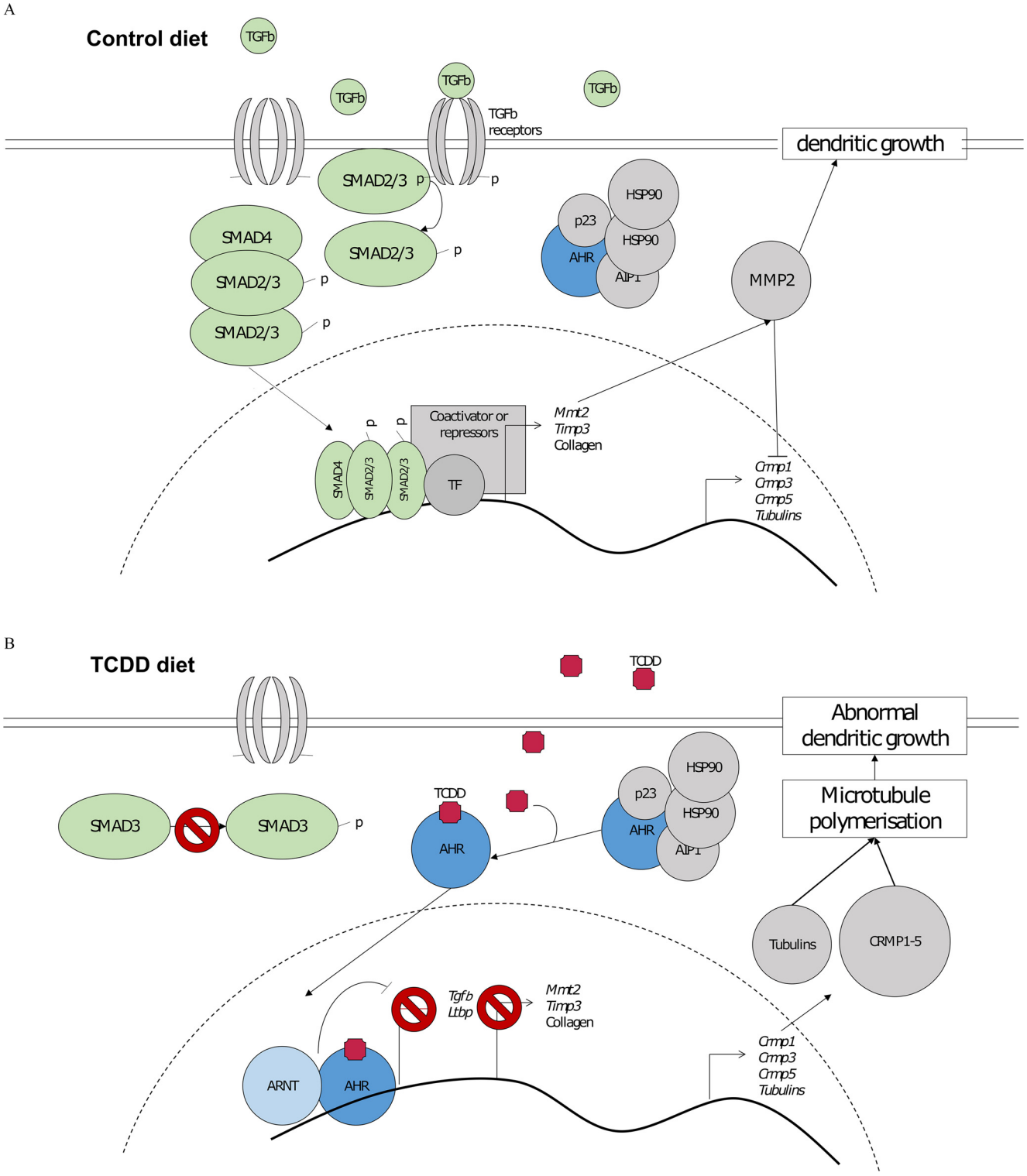

Figure 9. Possible mechanism of the disruption of dendritic branching in TCDD-exposed pyramidal neurons. (A) In the absence of TCDD, AHR is sequestered in the cytoplasm, bound to its chaperone complex. Binding of TGFβ ligands to the TGFβ receptors leads to phosphorylation of SMAD3 and SMAD2 and their translocation to the nucleus. SMAD2 and SMAD3 form a trimer with SMAD4 and drives gene expression of genes including Mmt2, Timp3, and collagen genes. MMP2 inhibits the expression and/or activity of Crmp genes. (B) In the presence of TCDD, AHR dissociates from the chaperone complex and translocates to the nucleus. The ligand-bound AHR forms a heterodimer with cofactors such as ARNT and inhibits the TGFβ pathway by repressing *TGF*β and/or Ltbp expression and/or SMAD3 activation, causing the down-regulation of TGFβ targets such as Mmp2 and ECM genes. In the absence of repression by MMP2, Crmp genes are up-regulated, and modulate arborization via direct interactions with microtubules. AHR, aryl hydrocarbon receptor; TCDD, 2,3,7,8 tetrachlorodibenzo-*p*-dioxin; TGF, transforming growth factor.

and of the use of embryos from the same litter per diet in our gene expression analysis.

In conclusion, we demonstrated that exposure to low amounts of TCDD in the diet during pregnancy can have significant effects on brain development lasting into adulthood. With many people around the world still exposed to TCDD levels exceeding the recommended tolerable intake of 2 pg/kg BW/wk, it is important to understand the possible neurodevelopmental effects. The observations presented in this manuscript emphasize the importance of considering the continued neurodevelopmental consequences of chronic exposure to the low amounts of TCDD persisting in the environment.

Acknowledgments

The authors are grateful to the Advanced Sequencing and Scientific Computing Facilities of The Francis Crick Institute. This work was supported by The Francis Crick Institute PhD Studentship, which receives funding from Cancer Research UK, the UK Medical Research Council, and Wellcome Trust. J.E. and J.P.L. are supported by the Ontario Brain Institute, the Canadian Institute for Health Research, and Brain Canada. We are also grateful to Dr. A. Bernhard at the Institute of Marine Research for assistance with the mouse diets.

A.K.L. was responsible for producing the mouse diets and the TCDD analyses. T.G. and Z.H. carried out the behavioral testing under the supervision of C.F. T.G. generated the fear conditioning data under the supervision of K.P.G. and K.M. J.E. and J.P.L. generated and analyzed the MRI data. T.G. and A.K.S. generated the CA1 morphology data. C.M., T.G., and C.H. analyzed the RNA sequencing data. S.H. carried out the statistical analysis of the CA1 morphology data, and T.G. carried out the rest of the statistical analysis. M.A.B. and C.F. designed and supervised the work, with contributions from C.H. and B.S. The manuscript was written by T.G. and M.A.B. with contributions from the other authors.

The data sets generated for the MRI and RNA sequencing experiments are available online as Excel Tables S3 and S6, respectively.

References

Aggleton JP, Christiansen K. 2015. The subiculum: the heart of the extended hippocampal system. Prog Brain Res 219:65–82, PMID: 26072234, https://doi.org/10.1016/bs.pbr.2015.03.003.

Anderson DR, Fisher R. 2002. Sources of dioxins in the United Kingdom: the steel industry and other sources. Chemosphere 46(3):371–381, PMID: 11829394, https://doi.org/10.1016/S0045-6535(01)00178-3.

Avants BB, Epstein CL, Grossman M, Gee JC. 2008. Symmetric diffeomorphic image registration with cross-correlation: evaluating automated labeling of elderly and neurodegenerative brain. Med Image Anal 12(1):26–41, PMID: 17659998, https://doi.org/10.1016/j.media.2007.06.004.

Avants BB, Tustison NJ, Song G, Cook PA, Klein A, Gee JC, et al. 2011. A reproducible evaluation of ANTs similarity metric performance in brain image registration. Neuroimage 54(3):2033–2044, PMID: 20851191, https://doi.org/10.1016/j.neuroimage.2010.09.025.

Aylsworth A, Jiang SX, Desbois A, Hou ST. 2009. Characterization of the role of full-length CRMP3 and its calpain-cleaved product in inhibiting microtubule polymerization and neurite outgrowth. Exp Cell Res 315(16):2856–2868, PMID: 19559021, https://doi.org/10.1016/j.yexcr.2009.06.014.

Aylward LL, Hays SM. 2002. Temporal trends in human TCDD body burden: decreases over three decades and implications for exposure levels. J Expo Anal Environ Epidemiol 12(5):319–328, PMID: 12198580, https://doi.org/10.1038/sj.jea.7500233.

Ayoub AE, Cai T-Q, Kaplan RA, Luo J. 2005. Developmental expression of matrix metalloproteinases 2 and 9 and their potential role in the histogenesis of the cerebellar cortex. J Comp Neurol 481(4):403–415, PMID: 15593342, https://doi.org/10.1002/cne.20375.

Bannerman DM, Niewoehner B, Lyon L, Romberg C, Schmitt WB, Taylor A, et al. 2008. NMDA receptor subunit NR2A is required for rapidly acquired spatial working memory but not incremental spatial reference memory. J Neurosci 28(14):3623–3630, PMID: 18385321, https://doi.org/10.1523/JNEUROSCI.3639-07.2008.

Beeler JA, Prendergast B, Zhuang X. 2006. Low amplitude entrainment of mice and the impact of circadian phase on behavior tests. Physiol Behav 87(5):870–880. PMID: 16600314, https://doi.org/10.1016/j.physbeh.2006.01.037.

Bell DR, Clode S, Fan MQ, Fernandes A, Foster PMD, Jiang T, et al. 2007. Toxicity of 2,3,7,8-tetrachlorodibenzo-p-dioxin in the developing male Wistar(Han) rat. II: chronic dosing causes developmental delay. Toxicol Sci 99(1):224–233, PMID: 17545211, https://doi.org/10.1093/toxsci/kfm141.

Bock KW. 2019. Aryl hydrocarbon receptor (AHR): from selected human target genes and crosstalk with transcription factors to multiple AHR functions. Biochem Pharmacol 168:65–70, PMID: 31228464, https://doi.org/10.1016/j.bcp.2019.06.015.

Bock NA, Nieman BJ, Bishop JB, Mark Henkelman R. 2005. In vivo multiple-mouse MRI at 7 Tesla. Magn Reson Med 54(5):1311–1316, PMID: 16215960, https://doi.org/10.1002/mrm.20683.

Brot S, Rogemond V, Perrot V, Chounlamountri N, Auger C, Honnorat J, et al. 2010. CRMP5 interacts with tubulin to inhibit neurite outgrowth, thereby modulating the function of CRMP2. J Neurosci 30(32):10639–10654, PMID: 20702696, https://doi.org/10.1523/JNEUROSCI.0059-10.2010.

Candland DK, Nagy M. 1969. The Open-Field: some comparative data. Ann NY Acad Sci 159(3):831–851, PMID: 4981885, https://doi.org/10.1111/j.1749-6632.1969.tb12982.x.

Caspersen IH, Aase H, Biele G, Brantsæter AL, Haugen M, Kvalem HE, et al. 2016a. The influence of maternal dietary exposure to dioxins and PCBs during pregnancy on ADHD symptoms and cognitive functions in Norwegian preschool children. Environ Int 94:649–660, PMID: 27424260, https://doi.org/10.1016/j.envint.2016.06.033.

Caspersen IH, Haugen M, Schjølberg S, Vejrup K, Knutsen HK, Brantsæter AL, et al. 2016b. Maternal dietary exposure to dioxins and polychlorinated biphenyls (PCBs) is associated with language delay in 3 year old Norwegian children. Environ Int 91:180–187, PMID: 26970589, https://doi.org/10.1016/j.envint.2016.02.031.

Chang X, Fan Y, Karyala S, Schwemberger S, Tomlinson CR, Sartor MA, et al. 2007. Ligand-independent regulation of transforming growth factor 1 expression and cell cycle progression by the aryl hydrocarbon receptor. Mol Cell Biol 27(17):6127–6139, PMID: 17606626, https://doi.org/10.1128/MCB.00323-07.

Cheng X, Haeberle S, Shytaj IL, Gama-Brambila RA, Theobald J, Ghafoory S, et al. 2020. NHC-gold compounds mediate immune suppression through induction of AHR-TGFβ1 signalling in vitro and in scurfy mice. Commun Biol 3(1): 10, PMID: 31909202, https://doi.org/10.1038/s42003-019-0716-8.

Chklovskii DB. 2004. Synaptic connectivity and neuronal morphology: two sides of the same coin. Neuron 43(5): 609–617, PMID: 15339643, https://doi.org/10.1016/j.neuron.2004.08.012.

Collins LL, Williamson MA, Thompson BD, Dever DP, Gasiewicz TA, Opanashuk LA, et al. 2008. 2,3,7,8-Tetracholorodibenzo-p-dioxin exposure disrupts granule neuron precursor maturation in the developing mouse cerebellum. Toxicol Sci 103(1):125–136, PMID: 18227101, https://doi.org/10.1093/toxsci/kfn017.

Collins DL, Neelin P, Peters TM, Evans AC. 1994. Automatic 3D intersubject registration of MR volumetric data in standardized Talairach space. J Comput Assist Tomogr 18(2):192–205, PMID: 8126267, https://doi.org/10.1097/00004728-199403000-00005.

Costa RM, Cohen D, Nicolelis MAL. 2004. Differential corticostriatal plasticity during fast and slow motor skill learning in mice. Curr Biol 14(13):1124–1134, PMID: 15242609, https://doi.org/10.1016/j.cub.2004.06.053.

Crawley JN. 2004. Designing mouse behavioral tasks relevant to autistic-like behaviors. Ment Retard Dev Disabil Res Rev 10(4):248–258, PMID: 15666335, https://doi.org/10.1002/mrdd.20039.

Crawley J, Goodwin FK. 1980. Preliminary report of a simple animal behavior model for the anxiolytic effects of benzodiazepines. Pharmacol Biochem Behav 13(2): 167–170, PMID: 6106204, https://doi.org/10.1016/0091-3057(80)90067-2.

Deacon RMJ. 2006. Digging and marble burying in mice: simple methods for in vivo identification of biological impacts. Nat Protoc 1(1):122–124, PMID: 17406223, https://doi.org/10.1038/nprot.2006.20.

deCatanzaro D. 2015. Sex steroids as pheromones in mammals: the exceptional role of estradiol. Horm Behav 68:103–116, PMID: 25125222, https://doi.org/10.1016/j.yhbeh.2014.08.003.

de la Parra J, Cuartero MI, Pérez-Ruiz A, García-Culebras A, Martín R, Sánchez-Prieto J, et al. 2018. AhR deletion promotes aberrant morphogenesis and synaptic activity of adult-generated granule neurons and impairs hippocampus-dependent memory. Eneuro 5(4):1–20, PMID: 30225360, https://doi.org/10.1523/eneuro.0370-17.2018.

Dever DP. 2013. *The Aryl Hydrocarbon Receptor and Cerebellar Granule Cell Neurogenesis: Implications for Development and Medulloblastoma Pathogenesis*. Doctoral thesis. http://hdl.handle.net/1802/28437 [accessed 8 May 2018].

Dever DP, Adham ZO, Thompson B, Genestine M, Cherry J, Olschowka JA, et al. 2016. Aryl hydrocarbon receptor (AhR) deletion in cerebellar granule neuron precursors impairs neurogenesis. Dev Neurobiol 76(5):533–550, PMID: 26243376, https://doi.org/10.1002/dneu.22330.

Dong X, Shen K, Bülow HE. 2015. Intrinsic and extrinsic mechanisms of dendritic morphogenesis. Annu Rev Physiol 77(1):271–300, PMID: 25386991, https://doi.org/10.1146/annurev-physiol-021014-071746.

Dorr AE, Lerch JP, Spring S, Kabani N, Henkelman RM. 2008. High resolution three-dimensional brain atlas using an average magnetic resonance image of 40 adult C57Bl/6J mice. Neuroimage 42(1):60–69, PMID: 18502665, https://doi.org/10.1016/j.neuroimage.2008.03.037.

Duong TD, Erickson CA. 2004. MMP-2 plays an essential role in producing epithelial-mesenchymal transformations in the avian embryo. Dev Dyn 229(1):42–53, PMID: 14699576, https://doi.org/10.1002/dvdy.10465.

EFSA CONTAM Panel (EFSA Panel on Contaminants in the Food Chain). 2018. Scientific opinion on the risk for animal and human health related to the presence of dioxins and dioxin-like PCBs in feed and food. EFSA J 16(11):5333, PMID: 32625737, https://doi.org/10.2903/j.efsa.2018.5333.

Emond C, Birnbaum LS, DeVito MJ. 2006. Use of a physiologically based pharmacokinetic model for rats to study the influence of body fat mass and induction of CYP1A2 on the pharmacokinetics of TCDD. Environ Health Perspect 114(9):1394–1400, PMID: 16966094, https://doi.org/10.1289/ehp.8805.

Endo T, Kakeyama M, Uemura Y, Haijima A, Okuno H, Bito H, et al. 2012. Executive function deficits and social-behavioral abnormality in mice exposed to a low dose of dioxin in utero and via lactation. PLoS One 7(12):e50741, PMID: 23251380, https://doi.org/10.1371/journal.pone.0050741.

Faqi AS, Dalsenter PR, Merker HJ, Chahoud I. 1998. Reproductive toxicity and tissue concentrations of low doses of 2,3,7,8-tetrachlorodibenzo-p-dioxin in male offspring rats exposed throughout pregnancy and lactation. Toxicol Appl Pharmacol 150(2):383–392, PMID: 9653070, https://doi.org/10.1006/taap.1998.8433.

Fernandes C, File SE. 1996. The influence of open arm ledges and maze experience in the elevated plus-maze. Pharmacol Biochem Behav 54(1):31–40, PMID: 8728536, https://doi.org/10.1016/0091-3057(95)02171-X.

Fernández M, Paradisi M, D'Intino G, Del Vecchio G, Sivilia S, Giardino L, et al. 2010. A single prenatal exposure to the endocrine disruptor 2,3,7,8-tetrachlorodibenzo-p-dioxin alters developmental myelination and remyelination potential in the rat brain. J Neurochem 115(4):897–909, PMID: 20807317, https://doi.org/10.1111/j.1471-4159.2010.06974.x.

Flanders KC, Lüdecke G, Engels S, Cissel DS, Roberts AB, Kondaiah P, et al. 1991. Localization and actions of transforming growth factor-beta s in the embryonic nervous system. Development 113(1):183–191, PMID: 1764993.

Friedel M, van Eede MC, Pipitone J, Chakravarty MM, Lerch JP. 2014. Pydpiper: a flexible toolkit for constructing novel registration pipelines. Front Neuroinform 8:67, PMID: 25126069, https://doi.org/10.3389/fninf.2014.00067.

Fukata Y, Itoh TJ, Kimura T, Ménager C, Nishimura T, Shiromizu T, et al. 2002. CRMP-2 binds to tubulin heterodimers to promote microtubule assembly. Nat Cell Biol 4(8):583–591, PMID: 12134159, https://doi.org/10.1038/ncb825.

Galani R, Jarrard LE, Will BE, Kelche C. 1997. Effects of postoperative housing conditions on spatial memory deficits in rats with selective lesions of either the hippocampus, subiculum or entorhinal cortex. Neurobiol Learn Mem 67(1):43–56, PMID: 9013500, https://doi.org/10.1006/nlme.1996.3745.

Genovese CR, Lazar NA, Nichols T. 2002. Thresholding of statistical maps in functional neuroimaging using the false discovery rate. Neuroimage 15(4):870–878, PMID: 11906227, https://doi.org/10.1006/nimg.2001.1037.

Gomez-Duran A, Carvajal-Gonzalez JM, Mulero-Navarro S, Santiago-Josefat B, Puga A, Fernandez-Salguero PM, et al. 2009. Fitting a xenobiotic receptor into cell homeostasis: how the dioxin receptor interacts with TGFbeta signaling. Biochem Pharmacol 77(4):700–712, PMID: 18812170, https://doi.org/10.1016/j.bcp.2008.08.032.

Gonthier B, Koncina E, Satkauskas S, Perraut M, Roussel G, Aunis D, et al. 2009. A PKC-dependent recruitment of MMP-2 controls semaphorin-3A growth-promoting effect in cortical dendrites. PLoS One 4(4):e5099, PMID: 19352510, https://doi.org/10.1371/journal.pone.0005099.

Gramatzki D, Pantazis G, Schittenhelm J, Tabatabai G, Köhle C, Wick W, et al. 2009. Aryl hydrocarbon receptor inhibition down-regulates the TGF-beta/Smad pathway in human glioblastoma cells. Oncogene 28(28):2593–2605, PMID: 19465936, https://doi.org/10.1038/onc.2009.104.

Granillo L, Sethi S, Keil KP, Lin Y, Ozonoff S, Iosif A-M, et al. 2019. Polychlorinated biphenyls influence on autism spectrum disorder risk in the MARBLES cohort. Environ Res 171:177–184, PMID: 30665119, https://doi.org/10.1016/j.envres.2018.12.061.

Haijima A, Endo T, Zhang Y, Miyazaki W, Kakeyama M, Tohyama C, et al. 2010. In utero and lactational exposure to low doses of chlorinated and brominated dioxins induces deficits in the fear memory of male mice. Neurotoxicology 31(4): 385–390, PMID: 20398696, https://doi.org/10.1016/j.neuro.2010.04.004.

Hildebrandt H, Müller S, Bussmann-Mork B, Goebel S, Eilers N. 2001. Are some memory deficits unique to lesions of the mammillary bodies? J Clin Exp Neuropsychol 23(4):490–501, PMID: 11780948, https://doi.org/10.1076/jcen.23.4.490.1234.

Hojo R, Stern S, Zareba G, Markowski VP, Cox C, Kost JT, et al. 2002. Sexually dimorphic behavioral responses to prenatal dioxin exposure. Environ Health Perspect 110(3):247–254, PMID: 11882475, https://doi.org/10.1289/ehp.02110247.

Ito M. 2000. Mechanisms of motor learning in the cerebellum. Brain Res 886(1–2):237–245, PMID: 11119699, https://doi.org/10.1016/S0006-8993(00)03142-5.

Ji Z, Zhang G, Chen L, Li J, Yang Y, Cha C, et al. 2018. Spastin interacts with CRMP5 to promote neurite outgrowth by controlling the microtubule dynamics. Dev Neurobiol 78(12):1191–1205, PMID: 30257070, https://doi.org/10.1002/dneu.22640.

Jonas P, Lisman J. 2014. Structure, function, and plasticity of hippocampal dentate gyrus microcircuits. Front Neural Circuits 8:107, PMID: 25309334, https://doi.org/10.3389/fncir.2014.00107.

Juricek L, Carcaud J, Pelhaitre A, Riday TT, Chevallier A, Lanzini J, et al. 2017. AhR-deficiency as a cause of demyelinating disease and inflammation. Sci Rep 7(1):1–9, PMID: 28851966, https://doi.org/10.1038/s41598-017-09621-3.

Kakeyama M, Endo T, Zhang Y, Miyazaki W, Tohyama C. 2014. Disruption of paired-associate learning in rat offspring perinatally exposed to dioxins. Arch Toxicol 88(3):789–798, PMID: 24292196, https://doi.org/10.1007/s00204-013-1161-y.

Kandasamy M, Lehner B, Kraus S, Sander PR, Marschallinger J, Rivera FJ, et al. 2014. TGF-beta signalling in the adult neurogenic niche promotes stem cell quiescence as well as generation of new neurons. J Cell Mol Med 18(7):1444–1459, PMID: 24779367, https://doi.org/10.1111/jcmm.12298.

Kim D, Pertea G, Trapnell C, Pimentel H, Kelley R, Salzberg SL, et al. 2013. TopHat2: accurate alignment of transcriptomes in the presence of insertions, deletions and gene fusions. Genome Biol 14(4):R36, PMID: 23618408, https://doi.org/10.1186/gb-2013-14-4-r36.

Kimura E, Kubo K-I, Matsuyoshi C, Benner S, Hosokawa M, Endo T, et al. 2015. Developmental origin of abnormal dendritic growth in the mouse brain induced by in utero disruption of aryl hydrocarbon receptor signaling. Neurotoxicol Teratol 52(pt A):42–50, PMID: 26526904, https://doi.org/10.1016/j.ntt.2015.10.005.

Kimura E, Endo T, Yoshioka W, Ding Y, Ujita W, Kakeyama M, et al. 2016. In utero and lactational dioxin exposure induces Sema3b and Sema3g gene expression in the developing mouse brain. Biochem Biophys Res Commun 476(2):108–113, PMID: 27178212, https://doi.org/10.1016/j.bbrc.2016.05.048.

Kimura E, Kubo K-I, Endo T, Ling W, Nakajima K, Kakeyama M, et al. 2017. Impaired dendritic growth and positioning of cortical pyramidal neurons by activation of aryl hydrocarbon receptor signaling in the developing mouse. PLoS One 12(8): e0183497, PMID: 28820910, https://doi.org/10.1371/journal.pone.0183497.

Kimura E, Tohyama C. 2018. Vocalization as a novel endpoint of atypical attachment behavior in 2,3,7,8-tetrachlorodibenzo-p-dioxin-exposed infant mice. Arch Toxicol 92(5):1741–1749, PMID: 29445839, https://doi.org/10.1007/s00204-018-2176-1.

Kishi R, Kobayashi S, Ikeno T, Araki A, Miyashita C, Itoh S, et al. 2013. Ten years of progress in the Hokkaido birth cohort study on environment and children's health: cohort profile - updated 2013. Environ Health Prev Med 18(6):429–450, PMID: 23959649, https://doi.org/10.1007/s12199-013-0357-3.

Kobayashi Y, Hirano T, Omotehara T, Hashimoto R, Umemura Y, Yuasa H, et al. 2015. Immunohistochemical analysis of 2,3,7,8-tetrachlorodibenzo-p-dioxin (TCDD) toxicity on the developmental dentate gyrus and hippocampal fimbria in fetal mice. J Vet Med Sci 77(11):1355–1361, PMID: 26096965, https://doi.org/10.1292/jvms.15-0238.

Koopman-Esseboom C, Weisglas-Kuperus N, de Ridder MA, Van der Paauw CG, Tuinstra LG, Sauer PJ, et al. 1996. Effects of polychlorinated biphenyl/dioxin exposure and feeding type on infants' mental and psychomotor development. Pediatrics 97(5):700–706, PMID: 8628610.

Lad HV, Liu L, Paya-Cano JL, Parsons MJ, Kember R, Fernandes C, et al. 2010. Behavioural battery testing: evaluation and behavioural outcomes in 8 inbred mouse strains. Physiol Behav 99(3):301–316, PMID: 19931548, https://doi.org/10.1016/j.physbeh.2009.11.007.

Landers JP, Bunce NJ. 1991. The Ah receptor and the mechanism of dioxin toxicity. Biochem J 276(2):273–287, PMID: 1646595, https://doi.org/10.1042/bj2760273.

Latchney SE, Hein AM, O'Banion MK, DiCicco-Bloom E, Opanashuk LA. 2013. Deletion or activation of the aryl hydrocarbon receptor alters adult hippocampal neurogenesis and contextual fear memory. J Neurochem 125(3):430–445, PMID: 23240617, https://doi.org/10.1111/jnc.12130.

Ledda F, Paratcha G. 2017. Mechanisms regulating dendritic arbor patterning. Cell Mol Life Sci 74(24):4511–4537, PMID: 28735442, https://doi.org/10.1007/s00018-017-2588-8.

Lee DH, Jacobs DR, Porta M. 2007. Association of serum concentrations of persistent organic pollutants with the prevalence of learning disability and attention deficit disorder. J Epidemiol Community Health 61(7):591–596, PMID: 17568050, https://doi.org/10.1136/jech.2006.054700.

Lerch JP, Carroll JB, Spring S, Bertram LN, Schwab C, Hayden MR, et al. 2008. Automated deformation analysis in the YAC128 Huntington disease mouse model. Neuroimage 39(1): 32–39, PMID: 17942324, https://doi.org/10.1016/j.neuroimage.2007.08.033.

Lerch JP, Sled JG, Henkelman RM. 2011. Magnetic Resonance Neuroimaging: Methods and Protocols. In: *MRI Phenotyping of Genetically Altered Mice*. Modo M, Bulte JWM, eds. Totowa, NJ: Humana Press, 349–361.

Li B, Liu H-Y, Dai L-J, Lu J-C, Yang Z-M, Huang L, et al. 2006. The early embryo loss caused by 2,3,7,8-tetrachlorodibenzo-p-dioxin may be related to the

accumulation of this compound in the uterus. Reprod Toxicol 21(3):301–306, PMID: 16257174, https://doi.org/10.1016/j.reprotox.2005.09.008.
Liao Y, Smyth GK, Shi W. 2014. FeatureCounts: an efficient general purpose program for assigning sequence reads to genomic features. Bioinformatics 30(7):923–930, PMID: 24227677, https://doi.org/10.1093/bioinformatics/btt656.
Longair MH, Baker DA, Armstrong JD. 2011. Simple Neurite Tracer: open source software for reconstruction, visualization and analysis of neuronal processes. Bioinformatics 27(17):2453–2454, PMID: 21727141, https://doi.org/10.1093/bioinformatics/btr390.
Love MI, Huber W, Anders S. 2014. Moderated estimation of fold change and dispersion for RNA-seq data with DESeq2. Genome Biol 15(12):550, PMID: 25516281, https://doi.org/10.1186/s13059-014-0550-8.
Lundebye A-K, Lock E-J, Rasinger JD, Nøstbakken OJ, Hannisdal R, Karlsbakk E, et al. 2017. Lower levels of persistent organic pollutants, metals and the marine omega 3-fatty acid DHA in farmed compared to wild Atlantic salmon (Salmo salar). Environ Res 155:49–59, PMID: 28189073, https://doi.org/10.1016/j.envres.2017.01.026.
Maranghi F, Tassinari R, Moracci G, Altieri I, Rasinger JD, Carroll TS, et al. 2013. Dietary exposure of juvenile female mice to polyhalogenated seafood contaminants (HBCD, BDE-47, PCB-153, TCDD): comparative assessment of effects in potential target tissues. Food Chem Toxicol 56:443–449, PMID: 23500779, https://doi.org/10.1016/j.fct.2013.02.056.
Maren S, Phan KL, Liberzon I. 2013. The contextual brain: implications for fear conditioning, extinction and psychopathology. Nat Rev Neurosci 14(6):417–428, PMID: 23635870, https://doi.org/10.1038/nrn3492.
Markowski VP, Cox C, Preston R, Weiss B. 2002. Impaired cued delayed alternation behavior in adult rat offspring following exposure to 2,3,7,8-tetrachlorodibenzo-p-dioxin on gestation day 15. Neurotoxicol Teratol 24(2):209–218, PMID: 11943508, https://doi.org/10.1016/S0892-0362(02)00186-1.
McBain CJ. 2008. Differential mechanisms of transmission and plasticity at mossy fiber synapses. Prog Brain Res 169:225–240, PMID: 18394477, https://doi.org/10.1016/S0079-6123(07)00013-1.
McFarlane HG, Kusek GK, Yang M, Phoenix JL, Bolivar VJ, Crawley JN. 2008. Autism-like behavioral phenotypes in BTBR T+tf/J mice. Genes Brain Behav 7(2):152–163, PMID: 17559418, https://doi.org/10.1111/j.1601-183X.2007.00330.x.
Mitsui T, Sugiyama N, Maeda S, Tohyama C, Arita J. 2006. Contextual fear conditioning-accompanied activation of cyclic AMP response element-binding protein in the hippocampal CA1 region of male rats. Neurosci Lett 398(3):206–210, PMID: 16442728, https://doi.org/10.1016/j.neulet.2005.12.087.
Morris RGM, Schenk F, Tweedie F, Jarrard LE. 1990. Ibotenate lesions of hippocampus and/or subiculum: dissociating components of allocentric spatial learning. Eur J Neurosci 2(12):1016–1028, PMID: 12106063, https://doi.org/10.1111/j.1460-9568.1990.tb00014.x.
Needham LL, Gerthoux PM, Patterson DG, Brambilla P, Smith SJ, Sampson EJ, et al. 1999. Exposure assessment: serum levels of TCDD in Seveso, Italy. Environ Res 80(2 pt 2):S200–S206, PMID: 10092434, https://doi.org/10.1006/enrs.1998.3928.
Nakajima S, Saijo Y, Kato S, Sasaki S, Uno A, Kanagami N, et al. 2006. Effects of prenatal exposure to polychlorinated biphenyls and dioxins on mental and motor development in Japanese children at 6 months of age. Environ Health Perspect 114(5):773–778, PMID: 16675436, https://doi.org/10.1289/ehp.8614.
Nakano N, Sakata N, Katsu Y, Nochise D, Sato E, Takahashi Y, et al. 2020. Dissociation of the AhR/ARNT complex by TGF-β/Smad signaling represses CYP1A1 gene expression and inhibits benze[a]pyrene-mediated cytotoxicity. J Biol Chem 295(27):9033–9051, PMID: 32409577, https://doi.org/10.1074/jbc.RA120.013596.
Nau H, Bass R, Neubert D. 1986. Transfer of 2,3,7,8-tetrachlorodibenzo-p-dioxin (TCDD) via placenta and milk, and postnatal toxicity in the mouse. Arch Toxicol 59(1):36–40, PMID: 3741141, https://doi.org/10.1007/BF00263955.
Negishi T, Shimomura H, Koyama T, Kawasaki K, Ishii Y, Kyuwa S, et al. 2006. Gestational and lactational exposure to 2,3,7,8-tetrachlorodibenzo-p-dioxin affects social behaviors between developing rhesus monkeys (Macaca mulatta). Toxicol Lett 160(3):233–244, PMID: 16125884, https://doi.org/10.1016/j.toxlet.2005.07.008.
Nguyen ATN, Nishijo M, Hori E, Nguyen NM, Pham TT, Fukunaga K, et al. 2013a. Influence of maternal exposure to 2,3,7,8-tetrachlorodibenzo-p-dioxin on socio-emotional behaviors in offspring rats. Environ Health Insights 7:1–14, PMID: 23493046, https://doi.org/10.4137/EHI.S10346.
Nguyen MN, Nishijo M, Nguyen ATN, Bor A, Nakamura T, Hori E, et al. 2013b. Effects of maternal exposure to 2,3,7,8-tetrachlorodibenzo-p-dioxin on parvalbumin- and calbindin-immunoreactive neurons in the limbic system and superior colliculus in rat offspring. Toxicology 314(1):125–134, PMID: 24060430, https://doi.org/10.1016/j.tox.2013.09.005.
Nieman BJ, Flenniken AM, Adamson SL, Henkelman RM, Sled JG. 2006. Anatomical phenotyping in the brain and skull of a mutant mouse by magnetic resonance imaging and computed tomography. Physiol Genomics 24(2):154–162, PMID: 16410543, https://doi.org/10.1152/physiolgenomics.00217.2005.
Nishijo M, Kuriwaki J-I, Hori E, Tawara K, Nakagawa H, Nishijo H, et al. 2007. Effects of maternal exposure to 2,3,7,8-tetrachlorodibenzo-p-dioxin on fetal brain growth and motor and behavioral development in offspring rats. Toxicol Lett 173(1):41–47, PMID: 17669605, https://doi.org/10.1016/j.toxlet.2007.06.007.
Nishijo M, Tai PT, Nakagawa H, Maruzeni S, Anh NTN, Van Luong H, et al. 2012. Impact of perinatal dioxin exposure on infant growth: a cross-sectional and longitudinal studies in dioxin-contaminated areas in Vietnam. PLoS One 7(7):e40273, PMID: 22815734, https://doi.org/10.1371/journal.pone.0040273.
Nishijo M, Pham TT, Nguyen ATN, Tran NN, Nakagawa H, Hoang LV, et al. 2014. 2,3,7,8-tetrachlorodibenzo-p-dioxin in breast milk increases autistic traits of 3-year-old children in Vietnam. Mol Psychiatry 19(11):1220–1226, PMID: 24637425, https://doi.org/10.1038/mp.2014.18.
Nowack N, Wittsiepe J, Kasper-Sonnenberg M, Wilhelm M, Schölmerich A. 2015. Influence of low-level prenatal exposure to PCDD/Fs and PCBs on empathizing, systemizing and autistic traits: results from the Duisburg Birth Cohort Study. PLoS One 10(6):e0129906–20, PMID: 26066795, https://doi.org/10.1371/journal.pone.0129906.
O'Mara S. 2006. Controlling hippocampal output: the central role of subiculum in hippocampal information processing. Behav Brain Res 174(2):304–312, PMID: 17034873, https://doi.org/10.1016/j.bbr.2006.08.018.
Park H-Y, Hertz-Picciotto I, Sovcikova E, Kocan A, Drobna B, Trnovec T, et al. 2010. Neurodevelopmental toxicity of prenatal polychlorinated biphenyls (PCBs) by chemical structure and activity: a birth cohort study. Environ Health 9(1):1–13, PMID: 20731829, https://doi.org/10.1186/1476-069X-9-51.
Peng L, Mayhew CN, Schnekenburger M, Knudsen ES, Puga A. 2008. Repression of Ah receptor and induction of transforming growth factor-β genes in DEN-induced mouse liver tumors. Toxicology 246(2–3):242–247, PMID: 18282651, https://doi.org/10.1016/j.tox.2008.01.002.
Pham NT, Nishijo M, Pham TT, Tran NN, Le VQ, Tran HA, et al. 2019. Perinatal dioxin exposure and neurodevelopment of 2-year-old Vietnamese children in the most contaminated area from Agent Orange in Vietnam. Sci Tot Environ 678:217–226, PMID: 31075589, https://doi.org/10.1016/j.scitotenv.2019.04.425.
Pham TT, Nishijo M, Nguyen ATN, Tran NN, Hoang LV, Tran AH, et al. 2015. Perinatal dioxin exposure and the neurodevelopment of Vietnamese toddlers at 1 year of age. Sci Total Environ 536:575–581, PMID: 26247686, https://doi.org/10.1016/j.scitotenv.2015.07.055.
Pokorný J, Yamamoto T. 1981. Postnatal ontogenesis of hippocampal CA1 area in rats. I. Development of dendritic arborisation in pyramidal neurons. Brain Res Bull 7(2):113–120, PMID: 7272792, https://doi.org/10.1016/0361-9230(81)90075-7.
Poland A, Glover E, Kende AS. 1976. Stereospecific, high affinity binding of 2,3,7,8-tetrachlorodibenzo-p-dioxin by hepatic cytosol. J Biol Chem 251(16):4936–4946, https://doi.org/10.1016/S0021-9258(17)33205-2.
Potvin O, Doré FY, Goulet S. 2009. Lesions of the dorsal subiculum and the dorsal hippocampus impaired pattern separation in a task using distinct and overlapping visual stimuli. Neurobiol Learn Mem 91(3):287–297, PMID: 18977452, https://doi.org/10.1016/j.nlm.2008.10.003.
Powers BE, Lin T-M, Vanka A, Peterson RE, Juraska JM, Schantz SL. 2005. Tetrachlorodibenzo-p-dioxin exposure alters radial arm maze performance and hippocampal morphology in female AhR +/- mice. Genes Brain Behav 4(1):51–59, PMID: 15660668, https://doi.org/10.1111/j.1601-183X.2004.00098.x.
Pirkle JL, Wolfe WH, Patterson DG, Needham LL, Michalek JE, Miner JC. 1989. Estimates of the half-life of 2,3,7,8-tetrachlorodibenzo-p-dioxin in Vietnam veterans of Operation Ranch Hand. J Toxicol Environ Health 27(2):165–171, PMID: 2733058, https://doi.org/10.1080/15287398909531288.
Rasinger JD, Carroll TS, Lundebye AK, Hogstrand C. 2014. Cross-omics gene and protein expression profiling in juvenile female mice highlights disruption of calcium and zinc signalling in the brain following dietary exposure to CB-153, BDE-47, HBCD or TCDD. Toxicology 321(1):1–12, PMID: 24680724, https://doi.org/10.1016/j.tox.2014.03.006.
Romano E, Michetti C, Caruso A, Laviola G, Scattoni ML. 2013. Characterization of neonatal vocal and motor repertoire of reelin mutant mice. PLoS One 8(5):e64407, PMID: 23700474, https://doi.org/10.1371/journal.pone.0064407.
Safe SH. 1998. Hazard and risk assessment of chemical mixtures using the toxic equivalency factor approach. Environ Health Perspect 106(suppl 4):1051–1058, PMID: 9703492, https://doi.org/10.1289/ehp.98106s41051.
Sarić N, Selby M, Ramaswamy V, Kool M, Stockinger B, Hogstrand C, et al. 2020. The AHR pathway represses TGFβ-SMAD3 signalling and has a potent tumour suppressive role in SHH medulloblastoma. Sci Rep 10(1):1–16, PMID: 31924815, https://doi.org/10.1038/s41598-019-56876-z.
Schantz SL, Seo B-W, Moshtaghian J, Peterson RE, Moore RW. 1996. Effects of gestational and lactational exposure to TCDD or coplanar PCBs on spatial learning. Neurotoxicol Teratol 18(3):305–313, PMID: 8725643, https://doi.org/10.1016/S0892-0362(96)90033-1.
Schantz SL, Bowman RE. 1989. Learning in monkeys exposed perinatally to 2,3,7,8-tetrachlorodibenzo-p-dioxin (TCDD). Neurotoxicol Teratol 11(1): 13–19, PMID: 2725437, https://doi.org/10.1016/0892-0362(89)90080-9.
Schindelin J, Arganda-Carreras I, Frise E, Kaynig V, Longair M, Pietzsch T, et al. 2012. FIJI: an open-source platform for biological-image analysis. Nat Methods 9(7):676–682, PMID: 22743772, https://doi.org/10.1038/nmeth.2019.

Schmidt EF, Strittmatter SM. 2007. The CRMP family of proteins and their role in Sema3A signaling. Adv Exp Med Biol 600:1–11, PMID: 17607942, https://doi.org/10.1007/978-0-387-70956-7_1.

Seo BW, Sparks AJ, Medora K, Amin S, Schantz SL. 1999. Learning and memory in rats gestationally and lactationally exposed to 2,3,7,8-tetrachlorodibenzo-p-dioxin (TCDD). Neurotoxicol Teratol 21(3):231–239, PMID: 10386826, https://doi.org/10.1016/S0892-0362(98)00049-X.

Seo BW, Powers BE, Widholm JJ, Schantz SL. 2000. Radial arm maze performance in rats following gestational and lactational exposure to 2,3,7,8-tetrachlorodibenzo-p-dioxin (TCDD). Neurotoxicol Teratol 22(4):511–519, PMID: 10974589, https://doi.org/10.1016/S0892-0362(00)00070-2.

Sholl D. 1953. Dendritic organization in the neurons of the visual and motor cortices of the cat. J Anat 87(4):387–406, PMID: 13117757.

Silginer M, Burghardt I, Gramatzki D, Bunse L, Leske H, Rushing EJ, et al. 2016. The aryl hydrocarbon receptor links integrin signaling to the TGF-β pathway. Oncogene 35(25):3260–3271, PMID: 26500056, https://doi.org/10.1038/onc.2015.387.

Smith DR, Gallagher M, Stanton ME. 2007. Genetic background differences and nonassociative effects in mouse trace fear conditioning. Learn Mem 14(9):597–605, PMID: 17823243, https://doi.org/10.1101/lm.614807.

Spencer Noakes TL, Henkelman RM, Nieman BJ. 2017. Partitioning k-space for cylindrical three-dimensional rapid acquisition with relaxation enhancement imaging in the mouse brain. NMR Biomed 30(11):e3802–13, PMID: 28902423, https://doi.org/10.1002/nbm.3802.

Spruston N. 2008. Pyramidal neurons: dendritic structure and synaptic integration. Nat Rev Neurosci 9(3):206–221, PMID: 18270515, https://doi.org/10.1038/nrn2286.

Steadman PE, Ellegood J, Szulc KU, Turnbull DH, Joyner AL, Henkelman RM, et al. 2014. Genetic effects on cerebellar structure across mouse models of autism using a magnetic resonance imaging atlas. Autism Res 7(1):124–137, PMID: 24151012, https://doi.org/10.1002/aur.1344.

Tai PT, Nishijo M, Kido T, Nakagawa H, Maruzeni S, Naganuma R, et al. 2011. Dioxin concentrations in breast milk of Vietnamese nursing mothers: a survey four decades after the herbicide spraying. Environ Sci Technol 45(15):6625–6632, PMID: 21718047, https://doi.org/10.1021/es201666d.

Tai PT, Nishijo M, Anh NTN, Maruzeni S, Nakagawa H, Van Luong H, et al. 2013. Dioxin exposure in breast milk and infant neurodevelopment in Vietnam. Occup Environ Med 70(9):656–662, PMID: 23390198, https://doi.org/10.1136/oemed-2012-101021.

Tai PT, Nishijo M, Nghi TN, Nakagawa H, Van Luong H, Anh TH, et al. 2016. Effects of perinatal dioxin exposure on development of children during the first 3 years of life. J Pediatr 175:159–166, PMID: 27189679, https://doi.org/10.1016/j.jpeds.2016.04.064.

Takaya R, Nagai J, Piao W, Niisato E, Nakabayashi T, Yamazaki Y, et al. 2017. CRMP1 and CRMP4 are required for proper orientation of dendrites of cerebral pyramidal neurons in the developing mouse brain. Brain Res 1655:161–167, PMID: 27836492, https://doi.org/10.1016/j.brainres.2016.11.003.

Thiel R, Koch E, Ulbrich B, Chahoud I. 1994. Peri- and postnatal exposure to 2,3,7,8-tetrachlorodibenzo-p-dioxin: effects on physiological development, reflexes, locomotor activity and learning behaviour in Wistar rats. Arch Toxicol 69(2):79–86, PMID: 7717865, https://doi.org/10.1007/s002040050141.

Tran NN, Pham TT, Ozawa K, Nishijo M, Nguyen ATN, Tran TQ, et al. 2016. Impacts of perinatal dioxin exposure on motor coordination and higher cognitive development in Vietnamese preschool children: a five-year follow-up. PLoS One 11(1):e0147655–15, PMID: 26824471, https://doi.org/10.1371/journal.pone.0147655.

Uchida Y, Ohshima T, Sasaki Y, Suzuki H, Yanai S, Yamashita N, et al. 2005. Semaphorin3A signalling is mediated via sequential Cdk5 and GSK3beta phosphorylation of CRMP2: implication of common phosphorylating mechanism underlying axon guidance and Alzheimer's disease. Genes Cells 10(2):165–179, PMID: 15676027, https://doi.org/10.1111/j.1365-2443.2005.00827.x.

Ullmann JFP, Watson C, Janke AL, Kurniawan ND, Reutens DC. 2013. A segmentation protocol and MRI atlas of the C57BL/6J mouse neocortex. Neuroimage 78:196–203, PMID: 23587687, https://doi.org/10.1016/j.neuroimage.2013.04.008.

Unkila M, Pohjanvirta R, Honkakoski P, Törrönen R, Tuomisto J. 1993. 2,3,7,8-Tetrachlorodibenzo-p-dioxin (TCDD) induced ethoxyresorufin-O-deethylase (EROD) and aldehyde dehydrogenase (ALDH3) activities in the brain and liver. A comparison between the most TCDD-susceptible and the most TCDD-resistant rat strain. Biochem Pharmacol 46(4):651–659, PMID: 8363638, https://doi.org/10.1016/0006-2952(93)90551-7.

Valentinuzzi VS, Buxton OM, Chang A-M, Scarbrough K, Ferrari EAM, Takahashi JS, et al. 2000. Locomotor response to an open field during C57BL/6J active and inactive phases: differences dependent on conditions of illumination. Physiol Behav 69(3):269–275, PMID: 10869592, https://doi.org/10.1016/S0031-9384(00)00219-5.

Vann SD, Aggleton JP. 2003. Evidence of a spatial encoding deficit in rats with lesions of the mammillary bodies or mammillothalamic tract. J Neurosci 23(8):3506–3514, PMID: 12716960, https://doi.org/10.1523/jneurosci.23-08-03506.2003

Verslegers M, Lemmens K, Van Hove I, Moons L. 2013. Matrix metalloproteinase-2 and -9 as promising benefactors in development, plasticity and repair of the nervous system. Prog Neurobiol 105:60–78, PMID: 23567503, https://doi.org/10.1016/j.pneurobio.2013.03.004.

Verslegers M, Van Hove I, Dekeyster E, Gantois I, Hu T-T, D'Hooge R, et al. 2015. MMP-2 mediates Purkinje cell morphogenesis and spine development in the mouse cerebellum. Brain Struct Funct 220(3):1601–1617, PMID: 24652381, https://doi.org/10.1007/s00429-014-0747-3.

Vigil FA, Mizuno K, Lucchesi W, Valls-Comamala V, Giese KP. 2017. Prevention of long-term memory loss after retrieval by an endogenous CaMKII inhibitor. Sci Rep 7(1):4040, PMID: 28642476, https://doi.org/10.1038/s41598-017-04355-8.

Von Hertzen LSJ, Giese KP. 2005. Memory reconsolidation engages only a subset of immediate-early genes induced during consolidation. J Neurosci 25(8):1935–1942, PMID: 15728833, https://doi.org/10.1523/JNEUROSCI.4707-04.2005.

Vorhees CV, Williams MT. 2014. Assessing spatial learning and memory in rodents. ILAR J 55(2):310–332, PMID: 25225309, https://doi.org/10.1093/ilar/ilu013.

Vreugdenhil HJI, Lanting CI, Mulder PGH, Boersma ER, Weisglas-Kuperus N. 2002. Effects of prenatal PCB and dioxin background exposure on cognitive and motor abilities in Dutch children at school age. J Pediatr 140(1):48–56, PMID: 11815763, https://doi.org/10.1067/mpd.2002.119625.

Widholm JJ, Seo B-W, Strupp BJ, Seegal RF, Schantz SL. 2003. Effects of perinatal exposure to 2,3,7,8-tetrachlorodibenzo-p-dioxin on spatial and visual reversal learning in rats. Neurotoxicol Teratol 25(4):459–471, PMID: 12798963, https://doi.org/10.1016/S0892-0362(03)00014-X.

Wolfe WH, Michalek JE, Miner JC, Pirkle JL, Caudill SP, Patterson DG, et al. 1994. Determinants of TCDD half-life in veterans of Operation Ranch Hand. J Toxicol Environ Health 41(4):481–488, PMID: 8145287, https://doi.org/10.1080/15287399409531858.

Yang M, Silverman JL, Crawley JN. 2011. Automated three-chambered social approach task for mice. Curr Protoc Neurosci 56(1):8.26.1–8.26.16, PMID: 21732314, https://doi.org/10.1002/0471142301.ns0826s56.

Yi JJ, Barnes AP, Hand R, Polleux F, Ehlers MD. 2010. TGF-β signaling specifies axons during brain development. Cell 142(1):144–157, PMID: 20603020, https://doi.org/10.1016/j.cell.2010.06.010.

Yoshimura T, Kawano Y, Arimura N, Kawabata S, Kikuchi A, Kaibuchi K, et al. 2005. GSK-3beta regulates phosphorylation of CRMP-2 and neuronal polarity. Cell 120(1):137–149, PMID: 15652488, https://doi.org/10.1016/j.cell.2004.11.012.

Yu C-Y, Gui W, He H-Y, Wang X-S, Zuo J, Huang L, et al. 2014. Neuronal and astroglial TGFβ-Smad3 signaling pathways differentially regulate dendrite growth and synaptogenesis. Neuromolecular Med 16(2):457–472, PMID: 24519742, https://doi.org/10.1007/s12017-014-8293-y.

Zaher H, Fernandez-Salguero PM, Letterio J, Sheikh MS, Fornace AJ, Roberts AB, et al. 1998. The involvement of aryl hydrocarbon receptor in the activation of transforming growth factor-β and apoptosis. Mol Pharmacol 54(2):313–321, PMID: 9687573, https://doi.org/10.1124/mol.54.2.313.

Zhang H-J, Liu Y-N, Xian P, Ma J, Sun Y-W, Chen J-S, et al. 2018. Maternal exposure to TCDD during gestation advanced sensory-motor development, but induced impairments of spatial learning and memory in adult male rat offspring. Chemosphere 212:678–686, PMID: 30176550, https://doi.org/10.1016/j.chemosphere.2018.08.118.